NASA Contractor Report 4427

IN-34
72160
P-58

Secondary Instability of High-Speed Flows and the Influence of Wall Cooling and Suction

Nabil M. El-Hady

NASA

Secondary Instability of High-Speed Flows and the Influence of Wall Cooling and Suction

Nabil M. El-Hady
Analytical Services & Materials, Inc.
Hampton, Virginia

NASA

SECONDARY INSTABILITY OF HIGH-SPEED FLOWS AND THE INFLUENCE OF WALL COOLING AND SUCTION

Nabil M. El-Hady †

Analytical Services and Materials, Inc.
Hampton, Virginia 23666

ABSTRACT

The periodic streamwise modulation of the supersonic and hypersonic boundary layers by a two-dimensional first-mode or second-mode wave makes the resulting base flow susceptible to a broad-band spanwise-periodic three-dimensional type of instability. The principal parametric resonance of this instability (subharmonic) has been analyzed using Floquet theory. The effect of Mach number and the effectiveness of wall cooling or wall suction in controlling the onset, the growth rate, and the vortical structure of the subharmonic secondary instability are assessed for both a first-mode and a second-mode primary wave. Results indicate that the secondary subharmonic instability of an insulated wall boundary layer is weakened as Mach number increases. Cooling of the wall destabilizes the secondary subharmonic of a second-mode primary wave, but stabilizes it when the primary wave is a first mode. Suction stabilizes the secondary subharmonic at all Mach numbers.

1. INTRODUCTION

Interest in boundary-layer transition of high Mach number flows has increased, and boundary-layer transition has become an important factor influencing the design of the hypersonic vehicle - its configuration, thermal protection system, and its engine requirements.

---

† Senior Scientist

Prediction and control of transition at high Mach numbers is extremely beneficial since skin friction and aerodynamic heating are considerably lower for laminar flows at high speeds.

For compressible and high-speed boundary-layer flows, the stability problem is more complex than for incompressible flows, and the direct relationship between instability and transition is unknown. A thermal boundary layer with mean density variations develops in addition to the velocity boundary layer, leading to changes in the distribution of the angular momentum through the boundary layer. Due to this, the generalized inflection point (the location in the boundary layer where the gradient of the product of density and vorticity is zero) moves toward the outer edge of the boundary layer as Mach number increases.

Compressibility is known to have a stabilizing effect on the primary wave, due to a change in the nature of the instability as Mach number increases. To describe the physical mechanism leading to the transition process in high-speed flows, the secondary instability approach is being used. This approach enables us to select the proper waves amongst a spectrum of amplified three-dimensional (3D) waves to model the nonlinear interaction.

Recent progress in the early nonlinear stage of transition, where strong three dimensionality takes place, has identified a major link in the transition process between the linear and fully nonlinear stages for incompressible boundary layers. It has shown that there is a well defined transition from laminar two-dimensional (2D) to laminar 3D waves through a secondary-instability mechanism. This mechanism has been reviewed for incompressible flows by Herbert [1] and Bayly et al. [2]. The extension of the secondary instability theory in a spatial form to compressible and high Mach number boundary-layer flows was examined by El-Hady [3-6], and Masad and Nayfeh [7], while Ng and Erlebacher [8] examined the temporal theory. The linear growth of a primary wave may parametrically excite a secondary growth with 3D character. This secondary instability may not lead to transition by itself, but as it grows, it interacts with both the mean flow and the primary wave, leading rapidly to transition.

At high speeds, the effect of cooling or suction in some of the early stages to transition needs to be fully assessed as means of transition control. This can serve the goal of optimizing

laminar flow control systems for supersonic and hypersonic vehicles. The effect of cooling or suction on the primary wave for high-speed flows depends on the type of instability in the boundary layer. This effect is well established in the literature, and it is briefly reviewed here. In the linear stage, and in the absence of cooling or suction, there exists one generalized inflection point in the compressible boundary layer. For subsonic and low supersonic boundary layers, the instability is of viscous type, and the most amplified disturbance is oblique, and is called the first mode. As the Mach number increases, the generalized inflection point moves toward the outer edge of the boundary layer until it disappears. With that, the viscous instability becomes weaker and the inviscid instability picks up. Consequently, the primary first-mode disturbance, which is dependent upon the presence of the generalized inflection point, is stabilized due to the change in the nature of the instability. Also, as Mach number increases, multiple eigenvalues of amplified and damped modes (Mack modes) appear in the solution of the compressible stability equations. The first of the Mack modes is called the second mode and is the most unstable of all the modes as a 2D disturbance. This mode is a high frequency, acoustical-type disturbance.

As the boundary layer is cooled or sucked, a second inflection point appears. Both inflection points move away from the wall and then disappear as the cooling or suction increases. When this happens, the primary first-mode disturbance is completely stabilized. The effect of wall cooling on the primary stability of boundary layers was one of the significant findings of Mack's calculations [9]. A primary first mode is strongly stabilized, and its most unstable frequency is decreased by cooling. In contrast, primary higher modes are destabilized by wall cooling, and the unstable frequency band shifts to higher values [10]. This means that a wave with fixed frequency may be stabilized by sufficient cooling, but the growth rate of the most amplified primary second mode increases quite rapidly with cooling. Malik's calculations [11] for transition prediction on sharp cones using the e^N method, showed that it is the first oblique mode and not the second mode that is responsible for transition up to about Mach number 7 (the first produces a higher value of N-factor than the second). This is

because, despite the fact that growth rates of the second mode are much higher, the streamwise extent of their region of instability is much shorter (producing lower value of N-factor). With wall cooling, the primary first mode is stabilized, while the primary second mode becomes more unstable with larger streamwise extent for a given second mode frequency. Consequently, as wall cooling increases, the second mode dominates the transition process, and its role becomes increasingly important at lower Mach numbers.

Suction is more effective in stabilizing the viscous instability, and, hence, it is more effective at low Mach numbers [11]. As Mach number increases, the minimum amount of suction needed to eliminate the generalized inflection point increases. The first mode is strongly stabilized by suction; on the other hand, suction loses its effectiveness in stabilizing the second mode at high Mach numbers [12]. With the increase in suction, the frequency of the most unstable second mode shifts to a higher value. Although a second mode with a fixed frequency may be destabilized by suction, the growth rates of the most unstable frequencies decrease quite rapidly.

The nonlinear evolution and breakdown in supersonic and hypersonic boundary layers, as well as the structure of the flow near transition, are still unknown. None of the high-speed stability experiments were designed to study these phenomena. However, a temporal direct numerical simulation (DNS) of parallel compressible boundary layers performed by Erlebacher and Hussaini [13] was able to unveil a secondary instability at Mach number 4.5 triggered by the interaction between a finite amplitude 2D wave with a 3D (first mode) disturbance. This instability was found to be weaker than those found in incompressible flows but qualitatively similar to the k-type breakdown. In a recent temporal DNS calculations of Mach 4.5 flow along a hollow cylinder, and Mach 6.8 flow along a 7 degree half-angle cone, Pruett and Zang [14] have confirmed that the subharmonic secondary instability is a viable path to transition in high-speed boundary-layer flow. On the other hand, with respect to the theoretical developments, the secondary instability theory was extended by the author [3-6] and by others [7,8] for compressible boundary layers.

In this paper, we study the linear secondary 3D instability of supersonic and high-speed flows. We investigate the effect of a small, but finite-amplitude, 2D or oblique compressible Tollmien-Schlichting (TS) wave on the growth of 3D perturbations in supersonic boundary layers, and the effect of small, but finite-amplitude, 2D second mode on the growth of 3D perturbations in hypersonic boundary layers. The study focuses on the growth of the secondary subharmonics due to their importance in a low disturbance environment. The influence of wall cooling and suction on the onset, growth rate, and the vortical structure of the secondary instability of the boundary layer is also investigated in order to assess their effectiveness as means of transition control at high speeds. Some early results of this work were described by the author elsewhere [6]. In section 2, the analysis is developed. Section 3 discusses the numerical procedures. Results and discussions are given in section 4. Then, we end with concluding remarks in section 5.

2. ANALYSIS

The flow field is described by the laminar compressible 3D Navier-Stokes and energy equations. Lengths, velocities, and time are made dimensionless using a reference length $L=(v_{0\infty}x/u_{0\infty})^{1/2}$, the free-stream velocity $u_{0\infty}$, and $L/u_{0\infty}$, respectively. Here, x is the distance from the leading edge of the flat plate and $v_{0\infty}$ is the kinematic viscosity coefficient evaluated at the free stream. The pressure is made dimensionless using $\rho_{0\infty} u_{0\infty}^2$. The temperature, density, specific heats, viscosity, and thermal conductivity of air (treated as perfect gas) are made dimensionless using their corresponding free-stream values. In terms of these dimensionless quantities and in a vectorial form, the governing equations read

$$\frac{\partial \rho}{\partial t}+\nabla.(\rho \mathbf{V}) = 0 \tag{1}$$

$$\frac{\partial(\rho \mathbf{V})}{\partial t}+\nabla.(\rho \mathbf{V}\mathbf{V}) = -\nabla p+\frac{1}{R}\nabla.\tau \tag{2}$$

$$\rho(\frac{\partial \theta}{\partial t}+\mathbf{V}.\nabla\theta) = (\hat{\gamma}-1)M_\infty^2 [\frac{\partial p}{\partial t}+\mathbf{V}.\nabla p+\frac{1}{R}\Phi] + \frac{1}{RP_r}\nabla.(\mu\nabla\theta) \tag{3}$$

with the state equation

$$\hat{\gamma} M_\infty^2 p = \rho \theta. \tag{4}$$

In the above equations, τ is the dimensionless viscous stress tensor, and Φ is the dimensionless dissipation function. They are defined as

$$\tau = \mu[\nabla V + (\nabla V)^T] + \lambda \nabla . V I \tag{5}$$

$$\Phi = \tau : \nabla V. \tag{6}$$

Also, $\hat{\gamma}$ is the ratio of specific heats, M_∞ is the free-stream Mach number, $R = \rho_{0\infty} u_{0\infty} L / \mu_{0\infty}$ is Reynolds number, $P_r = c_p \mu / k$ is Prandtl number, μ and λ are the first and second coefficients of viscosity, respectively, I is a unit tensor, and T denotes a transpose.

2.1. The Basic Flow

The basic flow consists of a 2D compressible locally parallel boundary layer modulated by a small, but finite-amplitude, compressible TS or oblique wave, here called the primary wave. The basic flow is assumed to be a solution of the equations of motion; it takes the form

$$\hat{q}(x,y,t) = q_0(y) + A [q_1(y) e^{i(\alpha_r x - \omega t)} + cc] + O(A^2) \tag{7}$$

where

$$A \equiv A(x) = A_0 e^{-\int \alpha_i dx} , \tag{8}$$

cc denotes a complex conjugate, and A_0 is an initial amplitude. For the spatial stability analysis, α is the complex wavenumber of the primary wave, defined as $\alpha = \alpha_r + i\alpha_i$, and ω is the frequency, which is real. We shall consider the variation of the primary amplitude, $A(x)$, in Eq (8) to be weak. This variation will be neglected, and A is assumed to be locally constant. Also, we shall neglect terms $O(A^2)$ in the analysis and assume that the 2D compressible flow is modulated only by a periodic component of the linear stability problem. Justification of these assumptions was considered in [5].

In Eq (7), q_0 stands for boundary-layer flow quantities $u_0, p_0, \theta_0, \rho_0,$ and μ_0, while q_1 stands for the eigensolutions of the primary wave; they are $u_1, v_1, p_1, \theta_1, \rho_1,$ and μ_1. These quantities represent velocities, pressure, temperature, density, and viscosity, respectively. Of course, y is the normal distance from the plate surface. With the assumption of constant pressure gradient across the mean boundary layer, the state equation relates the boundary-layer temperature and density profiles by

$$\rho_0 \theta_0 = 1 \tag{9}$$

and also relates the primary density disturbance to the temperature and pressure disturbances by

$$\hat{\gamma} M_\infty^2 \, p_1 = \rho_1 \theta_0 + \rho_0 \theta_1 + O(A^2) \tag{10}$$

The boundary-layer viscosity is related to the temperature through Sutherland's law, while the primary viscosity disturbance is assumed to be linearly related to the temperature disturbance by

$$\mu_1 = \frac{d\mu_0}{d\theta_0}\theta_1 + O(A^2). \tag{11}$$

The eigenfunctions, q_1, in Eq (7) are normalized such that the amplitude, A, of the primary wave measures directly the maximum root-mean-square value of the mass-flow disturbance in the flow direction. That is

$$\max_{0 \le y \le \infty} 2[m_1(y)]^2 = 1 \tag{12}$$

where m_1 is the mass-flow disturbance, given by

$$m_1 = \frac{u_0}{\theta_0} (\hat{\gamma} M_\infty^2 \, p_1 - \frac{\theta_1}{\theta_0}) + \frac{u_1}{\theta_0} \tag{13}$$

El-Hady [5] used the streamwise velocity perturbation to normalize the eigenfunctions, q_1. That choice was adequate for the low range of Mach numbers. As Mach number increases, the temperature disturbance increases rapidly, and the mass-flow disturbance seems more appropriate for this normalization.

The eigenfunctions of the primary wave are governed by a sixth-order system of equations for a 2D primary wave, or by eighth-order system of equations for a 3D primary wave.

2.2. The Secondary Instability

To study the linear 3D instability of the basic flow given by (7), we superpose a small unsteady disturbance on each velocity, thermodynamic, and transport quantity of the basic flow. That is, we let

$$q(x,y,z,t) = \hat{q}(x,y,t) + Bq_2(x,y,z,t) \tag{14}$$

where q_2 is a secondary disturbance eigenfunction that represents velocities u_2, v_2, w_2 in the x,y,z directions, pressure p_2, temperature θ_2, density ρ_2, and viscosity μ_2; they are normalized such that the amplitude, B, of the secondary disturbance measures the maximum root-mean-square value of the secondary mass-flow disturbance, m_2, which is given by

$$m_2 = \frac{u_0}{\theta_0} (\hat{\gamma} M_\infty^2 \, p_2 - \frac{\theta_2}{\theta_0}) + \frac{u_2}{\theta_0} + A \ (\rho_1 \bar{u}_2 + u_1 \bar{\rho}_2), \tag{15}$$

where the overbar indicates a complex conjugate. In a linear analysis, the amplitude, B, of the secondary disturbance is assumed small compared to the amplitude, A, of the primary wave in such a way that the primary will influence the modulation of the secondary, but not vice versa.

The basic flow given by (7) neglects the nonlinear distortion of the eigenfunction, q_1, at a finite amplitude of the primary wave. This has been justified in the incompressible secondary instability theory [1] on the basis that the 3D secondary instability occurs at small amplitudes of the primary wave, where the nonlinear distortion is weak. It was also noticed that the vortical nature of the 3D secondary instability is not affected by the nonlinearity. These justifications are still valid for the compressible secondary instability theory, if we accept the notion that compressibility will probably retard and attenuate any nonlinear distortion.

Equation (14) is substituted into Eqs (1-6), the basic flow is subtracted, and the resulting equations are linearized with respect to the secondary disturbance, q_2. We end up with five coupled partial differential equations for the secondary 3D instability. The coefficients of these

stability equations are functions of the basic flow and its derivatives, are independent of the spanwise coordinate z, and are periodic in x and t. Hence, the z-variation can be separated, and the Floquet theory of differential equations with periodic coefficients can be applied to give a solution to these equations in the form

$$q_2(x,y,z,t) = e^{\gamma x + \sigma t}\, e^{i\beta z}\, \tilde{\phi}(x,y,t) \tag{16}$$

where β is a real spanwise wavenumber of the secondary disturbance. It is a measure of the angle of divergence of the direction of propagation of the secondary disturbance from the primary-wave vector. Also, $\gamma = \gamma_r + i\gamma_i$ and $\sigma = \sigma_r + i\sigma_i$ are two complex characteristic exponents, and $\tilde{\phi}(x,y,t)$ is a periodic function of $(x - \omega t/\alpha)$, the same as the period of the basic flow. We express $\tilde{\phi}(x,y,t)$ in terms of Fourier series to obtain the following expression for $q_2(x,y,z,t)$

$$q_2(x,y,z,t) = e^{\gamma x + \sigma t} e^{i\beta z} \sum_{n=-\infty}^{\infty} \phi_n(y) e^{i n \alpha(x - \omega t/\alpha)}. \tag{17}$$

Equation (17) represents a general Floquet form for the eigenmodes of a periodic basic flow. The subharmonic and fundamental modes are special cases of this form. Given two values of the four real exponents, γ_r, γ_i, σ_r, and σ_i, in Eq (17), the solution of the resulting eigenvalue problem determines the other two values. For the purpose of our study of the spatial instability of subharmonic modes, we let γ_r represent the growth rate of the secondary distur-bance, $\sigma_r = 0$ (no temporal growth), $\sigma_i = -\omega/2$ for a pure subharmonic mode, and let γ_i represent the shift in the streamwise wavenumber of the secondary wave with respect to the primary one (detuned modes). A value of $\gamma_i = -\alpha/2$ means that the secondary disturbance is tuned with the basic state.

The truncation and convergence of the Fourier series in Eq (17) is important for the numerical results. For the incompressible flat-plate boundary layer, Herbert et al. [15] have shown that this series converges rapidly and the lowest truncation provides sufficient accuracy for practical purposes. Also, in their temporal compressible stability analysis, Ng and Erlebacher [8] have studied the convergence of the Fourier modes at $M_\infty = 1.6$, and at $M_\infty = 4.5$. They concluded that, for a 2D primary wave, the streamwise structure of the subharmonic

disturbance can be accurately captured by using only two Fourier modes just as in the incompressible flow.

For the spatial numerical treatment in this paper, the lowest possible truncation of Fourier series for subharmonic modes is used, that is

$$q_2(x,y,z,t) = e^{\gamma x} e^{i\beta z} [\phi_1(y)e^{\frac{1}{2}i(\alpha x - \omega t)} + \phi_{-1}(y)e^{-\frac{1}{2}i(\alpha x - \omega t)}] \tag{18}$$

When the secondary instability is tuned with the basic state, then $\phi_{-1} = \bar{\phi}_1$. Using Eq (18), the governing equations for the 3D subharmonic instability (governing ϕ_1) can be written in the form

$$(a\ D^2 + b\ D + c)\ \phi_1 = A(d\ D^2 + e\ D + f)\ \bar{\phi}_1 + O(A^2) \tag{19}$$

with a similar set of equations for ϕ_{-1}, where

$$\phi_1 \equiv (u_2, v_2, w_2, p_2, \theta_2)^T, \tag{20}$$

$D = d/dy$, and a, b, c, d, e, f are 5x5 matrices that are dependent upon the basic flow.

The density secondary disturbance, ρ_2, is related to the pressure secondary disturbance, p_2, by the state equation

$$\hat{\gamma}M_\infty^2\ p_2 = \rho_0\theta_2 + \theta_0\rho_2 + A(\rho_1\bar{\theta}_2 + \theta_1\bar{\rho}_2) + O(A^2), \tag{21}$$

while the viscosity secondary disturbance, μ_2, is related to the temperature secondary disturbance, θ_2, through a Taylor's expansion of the total viscosity that yields

$$\mu_2 = \frac{d\mu_0}{d\theta_0}\theta_2 + A\frac{d^2\mu_0}{d\theta_0^2}\theta_1\bar{\theta}_2 + O(A^2). \tag{22}$$

The system of Eqs (19) governs the spatial secondary 3D subharmonic instability of compressible 2D flows. They are five coupled ordinary differential equations for u_2, v_2, w_2, p_2, and θ_2. When supplemented with homogeneous boundary conditions, they constitute an eigenvalue problem in the form

$$\gamma = \Gamma(\alpha, \beta, R ; A) \tag{23}$$

for given boundary-layer velocity and temperature profiles, $u_0(y)$ and $\theta_0(y)$, respectively.

3. NUMERICAL PROCEDURES

The mean-flow equations (Appendix A) are numerically integrated by using a combination of a shooting technique and Runge-Kutta integrator. The thermodynamic and transport properties of the perfect gas are computed at each integration step as they vary with the temperature.

The primary instability which modulates the 2D compressible boundary layer is governed by six first-order sets of ordinary differential equations. They are numerically integrated as an initial value problem using a free-stream solution as the initial condition.

In this study, we limit our concern to the subharmonic instability that is tuned with the basic flow. The system of Eqs (18) may be written, by neglecting terms $O(A/R)$, as eight first-order complex equations in the form

$$DZ_n - \sum_{l=1}^{8} g_{nl} Z_l = A \sum_{l=1}^{8} h_{nl} \bar{Z}_l, \quad n = 1,2,..,8 \tag{24}$$

with the boundary conditions,

$$Z_1 = Z_3 = Z_5 = Z_7 = 0 \quad at \ y=0 \tag{25}$$

$$Z_1, Z_3, Z_5, Z_7 \rightarrow 0 \quad as \ y \rightarrow \infty \tag{26}$$

where

$$Z_1 = u_2, \ Z_2 = Du_2, \ Z_3 = v_2, \ Z_4 = p_2,$$

$$Z_5 = \theta_2, \ Z_6 = D\theta_2, \ Z_7 = w_2, \ Z_8 = Dw_2, \tag{27}$$

and g_{nl}, and h_{nl}, $n,l=1,2,..8$ are the elements of 8x8 variable coefficient matrices. They are given in Appendix B. While the g_{nl} are functions of the mean flow, frequency, and wavenumber of the subharmonic, the h_{nl} are functions of the basic flow parameters (including the primary wave).

We assume that the amplitude of the primary wave vanishes in the free stream at $y \geq y_e$, where e denotes the edge of the boundary layer. Then, the system (24) will have constant coefficients and can be solved analytically, producing four linearly independent, exponentially decaying solutions to conform with the boundary condition (26). With the free-stream solution as initial condition, Eqs (24) are integrated from $y=y_e$ to $y=0$ at the wall, using a variable step-size algorithm [16], based on the Runge-Kutta-Fehlburg fifth-order formulas. The step-size is adjusted during the integration process so as to keep an estimate of the local error per step below a specified tolerance. However, the acceptable solution is delivered at pre-assigned fixed grid in y.

A straightforward integration fails to produce four linearly independent solutions because of the buildup of parasitic errors among the different solutions. To overcome this difficulty, the integrator used is coupled with an orthonormalization test that is based on a modified Gram-Schmidt procedure. Since testing for independence after each integration step is expensive, we use a modified algorithm [17] and choose a preselected set of points where orthonormalization is performed. These points are assigned a priori with sufficient frequency by using information about the points where orthonormalization is needed. To obtain a nontrivial solution to the homogeneous equations (24) for a guessed eigenvalue, the eigensolution is normalized by the value of a nonvanishing perturbation quantity at the wall (e.g. Z_2, Z_4, Z_6, or Z_8). This is equivalent to imposing a nonhomogeneous boundary condition at the wall to avoid a trivial solution. At the wall, the values of the linearly independent solutions are linearly combined to satisfy all but one of the wall boundary conditions ($Z_7 = 0$). A Newton-Raphson technique is used to iterate on the eigenvalue to satisfy the missing wall boundary condition to within a specified accuracy of $O(10^{-5})$.

4. RESULTS AND DISCUSSION

Experiments indicate that the subharmonic instability mechanism leading to breakdown is favored when the amplitude of the primary wave is low or moderate, whereas the fundamental breakdown occurs for higher primary amplitudes. Because flight applications are mostly characterized by a low-disturbance background, the subharmonic 3D instability appears to be more realistic and more dangerous in such applications.

In a supersonic boundary layer, 3D primary waves become dominant, having an oblique angle about 40°–60° for the most unstable wave. The influence of the primary wave angle on the secondary growth rate was examined by Ng and Erlebacher [8] at Mach number 1.6. Their investigation was temporal and local. They concluded that the strongest subharmonic modes occur when the primary wave propagates in the mean-flow direction, and that they are tuned with the basic state (having the same phase velocity as the 2D primary wave). They also concluded that, with a primary-wave angle of 45°, the secondary subharmonic growth rate is much less than the 2D case, and that the first five Fourier modes, see Eq (18), are required to capture the secondary growth rate correctly.

For the previous reasons, we focus our study on the possibility of the formation of strong three dimensionality of the subharmonic type from purely 2D compressible basic flow. Results reported here show that a parametrical excitation by the finite amplitude primary wave will produce strong growth of secondary 3D subharmonics along a broad band of spanwise wavelengths. All reported results use a nondimensional frequency, F, defined as $F = 10^6 \omega / R$, and a spanwise wavenumber parameter, b, defined as $b = 10^3 \beta / R$. They represent a wave traveling downstream with a fixed physical frequency and with a fixed physical spanwise wavenumber.

In the next subsection, we study the insulated-wall boundary layer and discuss the effect of Mach number on: 1) the secondary instability growth rates, 2) the induced 3D vortical structure, 3) the mode shape of the secondary disturbances, and 4) the effect of the free stream temperature on the growth of the secondary subharmonics. In the following subsections, we

discuss the effect of wall cooling and the effect of suction. In these calculations, cooling or suction are applied through the entire boundary layer development. This is expected to influence both the mean flow and the amplitude of the primary wave. We will study the effect of wall cooling and suction both locally and globally. A local study means that both Reynolds number and the primary-wave amplitude are fixed (does not mean that cooling and suction are applied locally). This represents the influence of the mean flow modifications alone on the secondary subharmonics. However, the global effect of wall cooling and suction includes the effect of the change in the amplitude of the primary wave, as well as the increase in Reynolds number as the disturbance develops downstream.

4.1. Effect of Mach Number

Figure 1 compares the growth rates of the secondary subharmonic mode at Mach numbers 1.6, 2.2, 3.0, and 4.5 for an insulated wall boundary layer. Calculations are performed at a free-stream stagnation temperature $\theta_s = 311K$, and $R = 800$. The primary wave is 2D first mode with a frequency $F = 60$ and amplitude $A_m = 0.06$ (the subscript m refers to mass flow). The figure has basically the same features as subharmonic growth rates in incompressible [1, 18] and low Mach number [5] flows: the large values of the growth rates, the broad band of unstable subharmonics, and the sharp cutoff at low spanwise wavenumbers. The strong growth of the secondary subharmonics compared to that for the primary waves (which is $O(10^{-3})$ or less), especially in the region of interest where they are mostly unstable, justifies the assumption of neglecting the variation of the primary amplitude and considering it as locally constant (see Eq (8)).

At these conditions, Figure 1 indicates that compressibility has a stabilizing effect on the secondary subharmonic instability, with a considerable decrease in the growth rates and reduction in the unstable band of the spanwise wavenumbers as Mach number increases. It should be noted that at a fixed frequency, F, an increase in the Reynolds number and/or the amplitude

of the primary wave will result in an increase of the growth rates as well as the unstable band of the secondary subharmonics for all Mach numbers. At the local conditions of Figure 1, it seems that the mechanism of the secondary subharmonic instability, resulting from the parametric excitation by the finite-amplitude first-mode primary wave, is weakened as Mach number increases.

At different Mach numbers, Figure 2 shows the variation across the boundary layer of the root-mean-square values of the secondary subharmonic disturbance normalized with respect to m_2. The corresponding variations for the primary first-mode disturbances normalized with respect to m_1 are shown in the same figure for comparison. These calculations are performed at $R = 800$, $F=60$, $A_m = 0.06$, and $b=0.18$.

The location of the critical layer, indicated in Figure 2 by y_c, moves away from the wall as Mach number increases, followed by the peak amplitudes of all the primary and secondary disturbance quantities. At high Mach numbers, fluctuations take place near the edge of the boundary layer. In comparison with other secondary disturbance quantities, v_2 is very small, while the primary, v_1 disturbance has a considerable value. As Mach number increases, both the primary and secondary temperature disturbances increase rapidly, with a second peak developing near the wall for the primary disturbance. Both the streamwise and spanwise velocity components (u_2 and w_2) of the secondary disturbance, which have considerable amplitudes at low Mach numbers [5], diminish as Mach number increases. The figure also shows that the rate of decay of the secondary disturbances in the free stream is much faster than the rate of decay of the primary waves.

With the onset of the secondary instability, three-dimensionality is induced in the flow field, and the initial 2D vorticity of the base flow is deformed, producing a vortical structure. Figure 3(a) shows the spanwise vorticity contours of the total flow (the mean flow, the 2D primary wave, and the 3D secondary subharmonic) in the x-y plane at $z=0$ for several Mach numbers. The figure is plotted over four primary wavelengths, and for the amplitudes $A_m=B_m=0.06$ for the primary and secondary disturbances, respectively. The vortices are inclined

at an angle to the mean-flow direction. As Mach number increases, these vortices extend to and concentrate around the critical layer (the tick mark on the left side of each graph indicates the position of the critical layer). The spanwise velocity variations produce a streamwise vorticity shown in Figure 3(b) and plotted over two spanwise wavelengths in the $z-y$ plane at $x=0$, for the same Mach numbers. It shows counter-rotating vortices extending away from the wall toward the critical layer as Mach number increases. The interaction between the streamwise vorticity and the deformed spanwise component is the main drive to flow breakdown.

At high Mach numbers, a primary 2D second mode dominates the primary stage, and a parametrical excitation of its finite amplitude produces the growth of a secondary 3D subharmonic along a broad band of spanwise wavelengths. Figure 4 shows the growth rates of these secondary subharmonics at Mach numbers 4.5 and 7.0. These calculations are for a free-stream temperature $120K$ and $R = 1000$, and the primary wave is a 2D second mode with amplitude $A_m = 0.06$ and frequency $F = 200$ for $M_\infty = 4.5$, and $F = 180$ for $M_\infty = 7.0$.

The normalized variation across the boundary layer of both the secondary subharmonic and the primary wave is shown in Figure 5 for Mach numbers 4.5 and 7.0. Calculations are performed at the most unstable subharmonic spanwise wavenumbers corresponding to Figure 4. Figure 5 shows that the critical layer (y_c) moves toward the edge of the boundary layer as Mach number increases. Both the primary and the secondary temperature and mass flow disturbances have sharp peaks compared to their counterpart first mode in Figure 2. The v_2 disturbance is almost vanishing, while the induced spanwise velocity, w_2, disturbance is very small.

In spite of the weak growth of the subharmonic secondary instability at these hypersonic Mach numbers, the flow field is completely altered due to a vortical structure produced by the secondary instability. As shown in Figure 6, this structure is concentrated around the critical layer (the tick mark on the left side). The figure shows components of the angular momentum (the vorticity modulated by the mean density). The spanwise angular momentum is inclined to the mean-flow direction (Fig 6(a)), while the streamwise angular momentum shows counter rotating vortices (Fig 6(b)). Figure 6 is plotted over four primary streamwise wavelengths in

the x direction, over two subharmonic spanwise wavelengths in the z direction, and for the amplitudes $A_m = B_m = 0.06$ of the primary and secondary disturbances, respectively.

For the insulated-wall boundary layer, it is noted in Figure 7 that the free-stream temperature affects the growth rate of the secondary instability. The influence of the free-stream temperature, θ_∞, comes through the viscosity and the thermal conductivity of the mean flow and the primary wave. Figure 7(a) shows that at $M_\infty = 1.6$, the growth rate of the secondary subharmonic increases slightly with the increase in the free-stream temperature (the primary wave is a 2D first mode). Figure 7(b) shows the opposite; at $M_\infty = 4.5$, the growth rate of the secondary subharmonic decreases sharply with the increase of the free-stream temperature (the primary wave is a 2D second mode). Although our calculations at these conditions indicate that the growth rate of the primary wave (first mode or second mode) decreases as the free-stream temperature increases, results in Figures 7 are calculated for a fixed amplitude of the primary wave.

4.2. Effect of Wall Cooling

The effect of wall cooling on the subharmonic secondary instability is investigated at Mach numbers 0.8 and 1.6 using a 2D first-mode primary wave, and at Mach number 4.5 using a 2D second-mode primary wave. The wall cooling parameter, θ_w/θ_{ad}, is used for this purpose, where the suffixes w and ad refer to wall and adiabatic wall conditions, respectively. Cooling the wall influences both the mean flow and the amplitude of the primary wave. The net outcome depends largely on identifying the major disturbance in the flow field. First-mode and second-mode primary disturbances give opposite effects.

The local effect of cooling (both Reynolds number and the amplitude of the primary are fixed) is demonstrated at different Mach numbers in Figure 8. The figure shows that, whether the primary wave is a first mode (Figures 8(a) and 8(b)) or a second mode (Figure 8(c)), cooling can be stabilizing or destabilizing depending on the spanwise wavenumber of the secondary

subharmonic (a similar conclusion was reached by El-Hady [5] concerning the local effect of compressibility, which also can be stabilizing or destabilizing depending on the amplitude of the primary wave and the spanwise wavenumber of the secondary subharmonic).

At all Mach numbers in Figure 8, we notice that cooling shifts the most unstable spanwise wavenumber to a higher value and stabilizes it. The local effect of wall heating is shown to be stabilizing at low Mach numbers in contradiction with its known destabilizing effect. Wall heating effect is not investigated at higher Mach numbers since it is not practical; the adiabatic wall temperature is already high for metal structures.

Figures 9 and 10 show a comparison of the eigenfunctions of the secondary disturbance at different wall cooling levels at Mach numbers 1.6 and 4.5, respectively. In both figures, the v_2 component (not shown) is very small and is only slightly affected by wall cooling. Primary-wave eigenfunctions are also shown in both figures for comparison. Wall cooling tends to move the critical layer closer to the wall (the opposite occurs for wall heating), and the maximum amplitudes of both the primary and the secondary waves follow. This is true whether the primary is a first-mode wave (its growth rate decreases by cooling), or the primary is a second-mode wave (its growth rate increases by cooling). So, the stabilizing or destabilizing mechanism due to wall cooling does not depend on this fact. While the value of the maximum amplitude of the velocity components (u_2, w_2) is hardly affected by wall cooling (or heating), the temperature amplitude changes drastically. At $M_\infty = 4.5$, we notice an opposite effect of wall cooling on the two temperature peaks of the 2D second-mode primary wave. The wall peak is destabilized by cooling, while the outer peak is stabilized.

The vortical structure that appears in the flow field due to the secondary instability is affected by wall cooling or wall heating. At Mach number 1.6, Figure 11 shows that effect on the contours of the 2D-spanwise and 3D-spanwise angular momentums, that is before and after the onset of the secondary instability. Figure 12 shows the same effect on the contours of the 3D-spanwise and streamwise angular momentums at Mach number 4.5. These figures are plotted over four primary streamwise wavelengths in the x direction, over two secondary spanwise

wavelengths in the z direction, and for the amplitudes $A_m = B_m = 0.02$ for the primary and secondary disturbances, respectively. Notice that these figures show a local cooling effect where both R and A are fixed. This effect represents the influence of the mean-flow modification due to wall cooling on the components of the vortical structure. Regions of concentrated spanwise angular momentum are convected downstream, confining themselves near the wall, as the wall cooling level increases. The concentrated angular momentum follows the critical layer (tick mark on the y-axis) as wall cooling level changes. Figure 11 shows that wall heating at $M_\infty = 1.6$ has an opposite effect, where the vortical structure stretches away from the wall.

The local effect of wall cooling or heating has no practical value. To evaluate the overall effect on the onset and growth rate of the secondary 3D subharmonic, we should combine the effect of the change in the amplitude, A, of the primary wave, as well as the increase in R as the disturbances develop downstream. This is shown in Figures 13 and 14 at different Mach numbers. In these calculations, the initial amplitude of the primary wave is assumed at its first neutral point, and the spanwise wavenumber parameter, b, is held fixed. At Mach numbers 0.8 and 1.6 (Figures 13(a) and 13(b), respectively), we use a 2D first mode as a primary wave. These figures show that the total effect of wall cooling is to delay the onset of the secondary instability and to significantly decrease its growth rate. Heating has the opposite effect. Notice that while wall heating is locally stabilizing (see Figures 8(a) and 8(b), its overall effect is to completely destabilize the secondary subharmonic at these Mach numbers. In Figure 13, it is worth to notice the explosive growth rates of the 3D secondary subharmonic disturbances compared to the primary wave as Reynolds number increases. Also, with a cooling parameter 0.85 at $M_\infty = 0.8$, and with initial primary amplitude $A_{0m} = 0.0023$, the primary growth is almost zero, while (not shown in the figure) a considerable 3D growth takes place. At $M_\infty = 1.6$, and with initial primary amplitude $A_{0m} = 0.01$, the cooling parameter 0.8 overstabilizes the primary wave, yet large growth of the 3D secondary subharmonic takes place.

At $M_\infty = 4.5$, and for a second-mode primary wave, Figure 14 shows the effect of cooling on the primary wave as well as the overall effect of cooling on the onset and the growth rate

of the 3D secondary subharmonic. The figure emphasizes the known fact that the primary wave (second mode) is destabilized by cooling. The figure shows that, in spite of the delay in the onset of the 3D secondary subharmonic, its growth rate increases rapidly with wall cooling. Notice that at this Mach number the 3D growth is not explosive; it is of the same order as the primary wave when the initial amplitude of the primary, A_{0m}, is 0.01. The 3D growth increases as A_{0m} increases (shown in the figure for $A_{0m} = 0.03$), with the total effect of cooling still destabilizing. Figure 14 shows that, although the growth rates of the 3D subharmonic increases with wall cooling, the streamwise extent of the unstable region is reduced. A secondary amplification factor (we call it an S-factor) is defined as $S = \ln (B/B_0)$, with B_0 as the initial amplitude of the secondary disturbance. The S-factor is calculated and compared, in Figure 15, with the primary amplification factor (known as N-factor an defined as $N = \ln (A/A_0)$). The figure demonstrate clearly the overall destabilizing effect of wall cooling on both the primary wave and the secondary subharmonic at $M_\infty = 4.5$.

4.3. Effect of Suction

The similarity suction parameter, γ_0, defined in Appendix A, is used to investigate the effect of suction control on the secondary instability at Mach numbers 0.8, 1.6, and 4.5. Moderate suction of the boundary layer stabilizes the mean flow and reduces the amplitude of the primary wave.

Figure 16 demonstrate the local effect of suction (both Reynolds number and the amplitude of the primary wave are fixed) at $M_\infty = 0.8$, 1.6 (primary wave is a first mode), and $M_\infty = 4.5$ (primary wave is a second mode). They show the influence of the mean-flow modification by suction on the secondary subharmonic growth rates. Contrary to the findings in the previous section (Figure 8) of the mixed effect of wall cooling at fixed R and A, Figure 16 shows that suction, at fixed R and A, reduces the growth rate of the whole unstable band of the secondary

subharmonic and limits it to fewer unstable spanwise wavenumbers. These results are in harmony with previous results by El-Hady [18] on the effect of suction in controlling the secondary instability for incompressible boundary layers. Comparison of the incompressible results [18] and the results in Figures 16(a), and 16(b) show that the effectiveness of suction decreases as Mach number increases when the primary wave is a first mode. We notice that, while the most unstable spanwise wavenumber is hardly influenced by suction at Mach numbers 0.8 and 1.6 (in agreement with the incompressible results in [18]), the most unstable spanwise wavenumber becomes higher as suction level increases at Mach number 4.5, where the primary wave is a second mode. These results differ from the wall-cooling case where, at all Mach numbers, the most unstable spanwise wavenumber becomes higher as wall cooling increases.

Figure 17 shows the effect of suction on the eigenfunctions of both the primary and the secondary subharmonic at $M_\infty = 1.6$, where the primary is a 2D first mode. Figure 18 shows the effect of suction on a second-mode primary wave and the resulting secondary subharmonic. Suction, like wall cooling, tends to move the critical layer closer to the wall, followed by the peak amplitudes of both the primary and the secondary waves.

Figure 19 shows the effect of suction on the vortical structure at $M_\infty = 1.6$ before and after the onset of the secondary instability. The figure shows contours of the spanwise component of the angular momentum of the flow field. The contours are plotted over four primary wavelengths with amplitudes of the primary and secondary disturbances of equal magnitude. With suction, the concentrated spanwise angular momentum is confined nearer to the wall, following the critical layer.

The overall effect of suction, like wall cooling, on the onset and growth rate of the secondary instability incorporates the changes in both R and A as the disturbance develops downstream. Because the local effect of suction proved to be always stabilizing for different Reynolds numbers and primary amplitudes, we expect that the overall effect of suction is always stabilizing. Figures similar to 13(a) and 13(b) are expected at $M_\infty = 0.8$ and $M_\infty = 1.6$, but with suction instead of wall cooling.

At $M_\infty = 4.5$ and for a second mode primary wave, Figure 20 shows the effect of suction on the primary wave as well as the overall effect of suction on the onset and growth rate of the 3D secondary subharmonic. The figure emphasizes the known fact that the primary wave (second mode) is stabilized by suction. The figure shows that not only is the onset of the secondary subharmonic delayed by suction, but also the maximum growth rate is decreased and the streamwise extent of the subharmonic instability is reduced. Again, as we discussed before at this Mach number, the 3D growth is not explosive; it is of the same order as the primary wave when the initial amplitude of the primary $A_{0m} = 0.01$. The 3D growth increases as A_{0m} increases (shown in the figure for $A_{0m} = 0.03$), with the total effect of suction still stabilizing. This indicates that the S-factor will be significantly decreased by suction.

5. CONCLUDING REMARKS

We have investigated the principal parametric resonance of the spatial three-dimensional instability of high-speed boundary layers due to small, but finite-amplitude, two-dimensional, compressible Tollmien-Schlichting waves. Control of these early transition instabilities by wall cooling or suction is studied.

Computations performed for primary first- and second-mode waves show that the spatial growth rates of the induced secondary subharmonics are substantially weakened as Mach number increases. In spite of the weak growth of the secondary subharmonics at high Mach numbers, the flow field is completely altered by a vortical structure that is concentrated around the critical layer. The contrast between the explosive nature and the weak growth of the subharmonics at low and high Mach numbers, respectively, suggests that the secondary instability mechanism may hold a more significant and dominant role in the transition process as Mach number increases.

The normal component, v_2, of the secondary disturbance almost vanishes as Mach number increases. Both the streamwise and the spanwise velocity components of the secondary disturbance, which have a considerable amplitude at $M_\infty = 0$, decrease rapidly as Mach number

increases, affecting the production of the spanwise and the streamwise components of the angular momentum, respectively, and, hence, may be slowing the process of breakdown.

The free-stream temperature influences the growth rate of the secondary subharmonic. At $M_\infty = 1.6$, where the primary wave is a 2D first mode, the growth rate increases slightly with the increase in the free-stream temperature. At $M_\infty = 4.5$, where the primary wave is a 2D second mode, the growth rate decreases sharply with the increase in the free-stream temperature.

At the investigated Mach numbers, the local effect of wall cooling can be stabilizing or destabilizing depending on the spanwise wavenumber of the secondary subharmonic. But the most unstable spanwise wavenumber is stabilized and shifted to a higher value as wall cooling increases. On the other hand, the local effect of suction is always stabilizing, the growth rates of the secondary subharmonics are reduced, and the band of unstable spanwise wavenumbers is narrowed. The most unstable spanwise wavenumber is not influenced by suction at low Mach numbers, but it becomes higher as suction level increases at $M_\infty = 4.5$, where the primary wave is a second mode.

Practically, the overall effect of compressibility, wall cooling, or suction includes the changes in Reynold number and the primary-wave amplitude as any instability wave develops downstream. When these changes are incorporated into the calculations, compressibility was shown here and in [5] to stabilize the secondary subharmonic instability. Also, suction is shown to stabilize the secondary instability, due to a first- or a second-mode primary wave. The onset of the instability is delayed, the growth rates are reduced, and the streamwise extent of the instability is narrowed.

The overall effect of cooling is also shown to stabilize the secondary instability in the same way suction does at low Mach numbers, where the primary wave is a first mode. At higher Mach numbers, where the primary wave is a second mode, wall cooling does delay the onset of the secondary instability and narrows its streamwise extent, but the growth rate of the secondary subharmonic increases rapidly, resulting in a higher S-factor and thus destabilizing the boundary layer.

ACKNOWLEDGMENT

APPENDIX A: The Compressible Mean Flow

The 2D compressible boundary-layer equations for zero pressure gradient and with suction and heat transfer are reduced to the following set of ODE's and boundary conditions:

$$(\rho\mu u')' + g u' - \gamma_0 u' = 0$$

$$(\rho\mu\theta'/P_r)' + g\theta' + 2\rho\mu u'^2 - \gamma_0\theta' = 0$$

$$g' - \frac{1}{2}\rho u = 0$$

$$u = 0, \quad g = 0, \quad \theta' = 0 \quad or \quad \theta = \theta_w \quad at \quad \eta = 0$$

$$u \to 1, \quad \theta \to 0 \quad as \quad \eta \to \eta_e$$

by using the transformation

$$\eta = \frac{(R_x)^{1/2}}{x} \int_0^y \rho \, dy$$

as well as a stream function to satisfy the continuity equation. Here, R_x is the free-stream x–Reynolds number, ρ is the density, x is the distance along the plate, y is the distance normal to it, and

$$\theta = \frac{h - h_e}{h_{oe} - h_e}, \qquad \gamma_0 = \frac{\rho_w v_w}{\rho_\infty U_\infty}(R_x)^{1/2},$$

where h and h_o are the fluid enthalpy and the stagnation enthalpy, respectively, e and w denote conditions at the edge of the boundary layer and at the wall, respectively, and γ_0 is the similarity suction parameter.

The variation of the viscosity, μ, and thermal conductivity, k, of the perfect gas with temperature θ are given in [4]. For the variation of the enthalpy and Prandtl number with

temperature, the NBS perfect gas tables are used. The specific heat, c_p, is computed from the definition of Prandtl number using the calculated values of μ and k and the tabulated values of P_r.

APPENDIX B: Nonzero Elements of Matrices g and h in Eq (24)

$g_{12} = 1$,

$g_{21} = R\nabla/(\mu_0\theta_0) - \Lambda^2 + \beta^2$, $\quad g_{22} = -\mu_0'/\mu_0$,

$g_{23} = Ru_0'/(\mu_0\theta_0) - \Lambda(\mu_0'/\mu_0 + m_1\theta_0'/\theta_0)$,

$g_{24} = \Lambda(R/\mu_0 + m_1\hat{\gamma}M_\infty^2\nabla)$,

$g_{25} = -(\hat{\mu}_0 u_0')'/\mu_0 - m_1\Lambda\nabla/\theta_0$, $\quad g_{26} = -\hat{\mu}_0 u_0'/\mu_0$,

$g_{31} = -\Lambda$, $\quad g_{33} = \theta_0'/\theta_0$, $\quad g_{34} = -\hat{\gamma}M_\infty^2\nabla$,

$g_{35} = \nabla/\theta_0$, $\quad g_{37} = -\beta$

$g_{41} = \chi\Lambda[m\mu_0' + m_2(\mu_0\theta_0'/\theta_0 - \mu_0')]/R$,

$g_{42} = \chi\Lambda\mu_0(m_1 + m_2)/R$

$g_{43} = \chi[\mu_0(\Lambda^2 - \beta^2) - \nabla/\theta_0]/R$

$g_{44} = \chi\hat{\gamma}M_\infty^2 m_2[-\mu_0'\nabla + \mu_0(\theta_0'\nabla/\theta_0 - \Lambda u_0')]$

$g_{45} = \chi[\Lambda u_0'\hat{\mu}_0 + m_2(\mu_0'\nabla + \mu_0 u_0'\Lambda)/\theta_0]/R$

$g_{46} = \chi m_2\mu_0\nabla/(R\theta_0)$

$g_{47} = \chi[m\beta\mu_0' - m_2\beta(\mu_0' + \mu_0\theta_0'/\theta_0)]/R$

$g_{48} = -\chi\beta\mu_0/R$

$g_{56} = 1$

$g_{62} = -2(\hat{\gamma}-1)M_\infty^2 P_r u_0'$,

$g_{63} = RP_r\theta_0'/(\mu_0\theta_0) - 2(\hat{\gamma}-1)M_\infty^2 P_r\Lambda u_0'$

$g_{64} = -R(\hat{\gamma}-1)M_\infty^2 P_r \nabla/\mu_0,$

$g_{65} = RP_r \nabla/(\mu_0\theta_0) - (\hat{\gamma}-1)M_\infty^2 P_r \hat{\mu}_0 u_0'^2/\mu_0 - \Lambda^2 + \beta^2 - (\hat{\mu}_0\theta_0'' + \mu_0^+\theta_0'^2)/\mu_0$

$g_{66} = -2\mu_0'/\mu_0$

$g_{78} = 1$

$g_{83} = \beta(\mu_0'/\mu_0 + m_1\theta_0'/\theta_0)$

$g_{84} = \beta(m_1\hat{\gamma}M_\infty^2\nabla - R/\mu_0), \quad g_{85} = \beta m_1\nabla/\theta_0$

$g_{87} = g_{21}, \quad g_{88} = g_{22}$

$h_{21} = R(\Lambda u_1/\theta_0 + \overline{\nabla}\rho_1)/\mu_0, \quad h_{22} = Rv_1/(\mu_0\theta_0)$

$h_{23} = R(u_1'/\theta_0 + u_0'\rho_1)/\mu_0$

$h_{24} = -R\hat{\gamma}M_\infty^2[i(\omega-\alpha_r u_0)u_1 - u_0'v_1]/(\mu_0\theta_0),$

$h_{25} = -h_{24}/(\hat{\gamma}M_\infty^2\theta_0)$

$h_{31} = -\rho_1 i\alpha_r\theta_0, \quad h_{33} = -\theta_0(\rho_1' + \rho_1\theta_0''/\theta_0) + \hat{\gamma}M_\infty^2\overline{\nabla}v_1/\theta_0$

$h_{34} = \hat{\gamma}M_\infty^2(\theta_0\rho_1\overline{\nabla} + \theta_0'v_1/\theta_0 + \nabla\theta_1/\theta_0 - \Lambda u_1 - v_1')$

$h_{35} = -\rho_1\overline{\nabla} - 2\theta_0'v_1/\theta_0^2 + (\rho_1 - \theta_1/\theta_0^2)\nabla + (\Lambda u_1 + v_1')/\theta_0$

$h_{36} = v_1/\theta_0$

$h_{41} = -\chi[i\alpha_r - (\gamma_r - \frac{1}{2}i\alpha_r)]v_1/\theta_0$

$h_{43} = -\chi[(\gamma_r - \frac{1}{2}i\alpha_r)u_1/\theta_0 + v_1'/\theta_0 + \overline{\nabla}\rho_1 + \theta_0'v_1/\theta_0^2]$

$h_{44} = \chi\hat{\gamma}M_\infty^2[i(\omega - \alpha_r u_0) + \nabla]v_1/\theta_0$

$h_{45} = -h_{44}/(\hat{\gamma}M_\infty^2\theta_0), \quad h_{47} = \chi\beta_r v_1/\theta_0$

$h_{61} = RP_r i\alpha_r[\theta_1/\theta_0 - (\hat{\gamma}-1)M_\infty^2 p_1]\mu_0$

$$h_{63} = RP_r[\theta_1'/\theta_0 + \rho_1\theta_0' - (\hat{\gamma}-1)M_\infty^2 p_1' - \overline{\nabla}v_1/\theta_0]/\mu_0$$

$$h_{64} = -R\,(\hat{\gamma}-1)M_\infty^2 P_r(\gamma_r - \tfrac{1}{2}i\,\alpha_r)u_1/\mu_0 + \hat{\gamma}M_\infty^2 RP_r[-i\,(\omega-\alpha_r u_0)\theta_1 + \theta_0'v_1]/(\mu_0\theta_0)$$

$$h_{65} = RP_r[(\gamma_r - \tfrac{1}{2}i\,\alpha_r)u_1/\theta_0 + \rho_1\overline{\nabla} + i\,(\omega-\alpha_r u_0)\theta_1 - \theta_0'v_1)/\theta_0^2]/\mu_0$$

$$h_{66} = RP_r v_1/(\mu_0\theta_0)$$

$$h_{87} = R\,[(\gamma_r - \tfrac{1}{2}i\,\alpha_r)u_1/\theta_0 + \overline{\nabla}\rho_1]/\mu_0$$

$$h_{88} = Rv_1/(\mu_0\theta_0)$$

Here, $m = 2(e-1)/3$ is the ratio of the second viscosity coefficient, λ_0, to the first viscosity coefficient, μ_0; $e=0$ corresponds to the Stokes hypothesis, but it is taken as 0.8 in this analysis. Also, $m_1=m+1$, $m_2=m+2$, $\hat{\mu}_0=d\mu_0/d\theta_0$, $\mu_0^+=d\hat{\mu}_0/d\theta_0$, and,

$$\Lambda = \gamma_r + \tfrac{1}{2}i\,\alpha_r$$

$$\nabla = \Lambda u_0 + \sigma_i - \tfrac{1}{2}i\,\omega$$

$$\chi = 1/(1 + m_2\,\mu_0\hat{\gamma}M_\infty^2\nabla/R)$$

$$\rho_1 = (\hat{\gamma}M_\infty^2\,p_1 - \theta_1/\theta_0)/\theta_0$$

REFERENCES

1. Herbert, Th.: Secondary Instability of Boundary Layers, Ann. Rev. Fluid Mech., vol. 20, 1988, pp. 487-526.

2. Bayly, B. J.; Orszag, S. A. and Herbert, Th.: Instability Mechanisms in Shear-Flow Transition, Ann. Rev. Fluid Mech., vol. 20, 1988, pp. 359-391.

3. El-Hady, N. M.: Secondary Three-Dimensional Instability in Compressible Boundary Layers. Transonic Symposium: Theory, Application, and Experiment, NASA CP-3020, vol. I, part 2,

1988, pp. 691-704.

4. El-Hady, N. M.: Secondary Instability of Compressible Boundary Layer to Subharmonic Three-Dimensional Disturbances. AIAA Paper No. 89-0035, 1989; also NASA CR-4251, September 1989.

5. El-Hady, N. M.: Spatial Three-Dimensional Secondary Instability of Compressible Boundary-Layer Flows. AIAA J. vol. 29 (5), May 1991, pp. 688-696.

6. El-Hady, N. M.: Secondary Instability of High-Speed Flows and the Influence of Wall Cooling and Suction. AIAA Paper 91-1647, 1991.

7. Masad, J., A.; and Nayfeh, A. H.: Subharmonic Instability of Compressible Boundary Layers. Phys. Fluids A, vol. 2, 1990.

8. Ng, L. L.; and Erlebacher, G.: Secondary Instabilities in Compressible Boundary Layers. ICASE Report No.90-58, submitted to Phys. Fluids.

9. Mack, L. M.: Review of Linear Compressible Stability Theory. In Stability for Time Dependent and Spatially Varying Flows, ed. D. L. Dwoyer and M. Y. Hussaini, 1985, pp. 164-187, Springer-Verlag, New York.

10. Lysenko, V. I.; and Maslov, A. A.: The Effect of Cooling on Supersonic Boundary-Layer Stability. J. Fluid Mech., vol. 147, 1984, p 39.

11. Malik, M. R.: Prediction and Control of Transition in Hypersonic Boundary Layers. AIAA Paper 87-1414, 1987.

12. Al-Maaitah, A. A.; and Nayfeh, A. H.: Effect of Suction on the Stability of Supersonic and Hypersonic Boundary Layers. Proc. Int. Conf. Fluid Mech. 3, Cairo, Egypt, January 2-4, 1990, vol. 2, p 677.

13. Erlebacher, G.; and Hussaini, M. Y.: Stability and Transition in Supersonic Boundary Layer. AIAA Paper 87-1416, 1987.

14. Pruett, C. D.; and Zang, T. A.: Direct Numerical Simulation of Laminar Breakdown in High-Speed Axisymmetric Boundary Layer. AIAA Paper 92-0742, 1992.

15. Herbert, Th.; Bertolotti, F. P.; and santos, G. R.: Floquet Analysis of Secondary Instability in Shear Flows. In Stability of Time-Dependent and Spatially Varying Flows, ed. D. L. Dwoyer, M. Y. Hussaini, p 43, 1986, Springer-Verlag, New York.

16. Scott. M. R. and Watts, H. A.: Computational Solution of Linear Two- Point Boundary-Value Problems Via Orthonormalization. SIAM J. Numer. Anal., vol. 14, 1977, pp.40-70.

17. Darlow, B. L.; Scott, M. R.; and Watts, H. A.: Modifications of SUPORT, a linear Boundary-Value Problems Via Orthonormalization. SIAM J. Numer. Anal., vol. 14, p 40, 1977.

18. El-Hady, N. M.: Effect of Suction on Controlling the Secondary Instability of Boundary Layers. NASA CR-4306, July 1990; also Phys. Fluids A, vol. 3, March 1991.
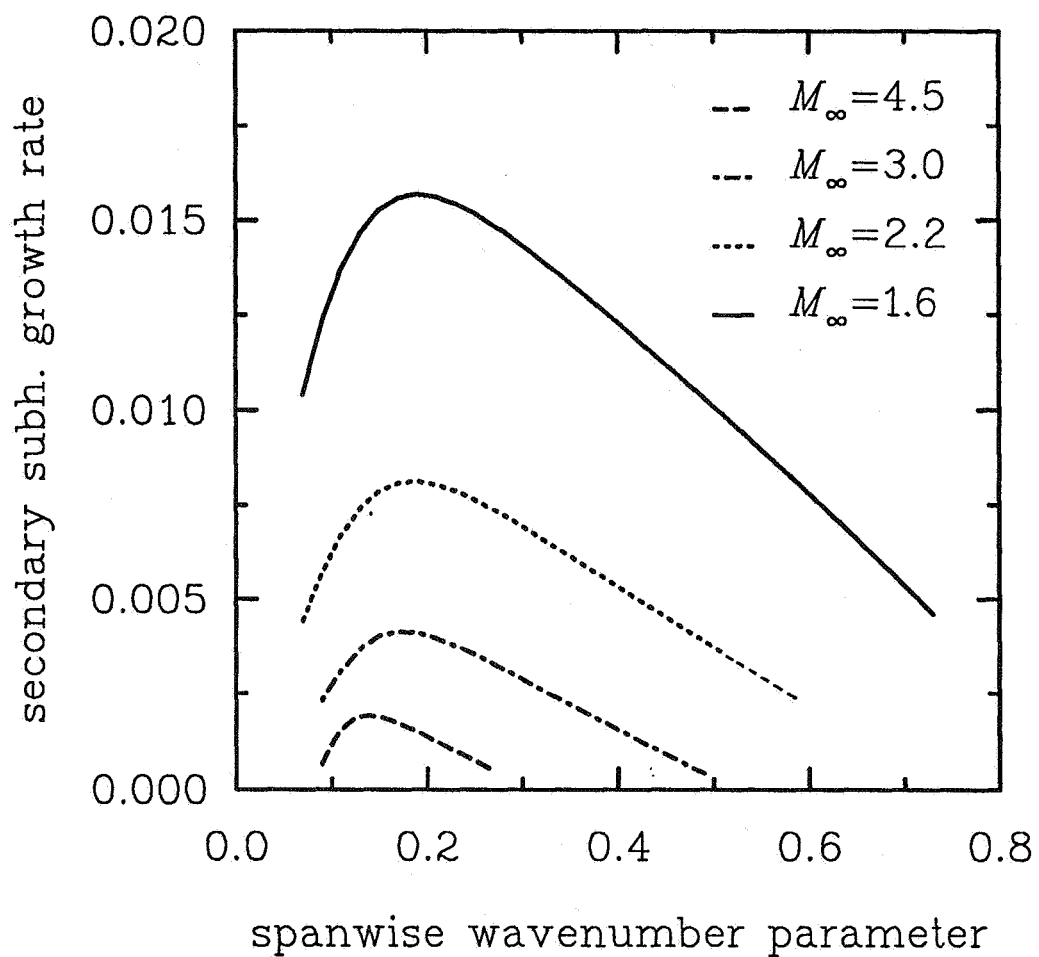
Figure 1 Effect of Mach Number on the growth rate and the unstable band of the spanwise wavenumbers of the secondary subharmonics at $R = 800$, $F = 60$, $A_m = 0.06$, and $\theta_s = 311K$. The primary wave is a 2D first mode.
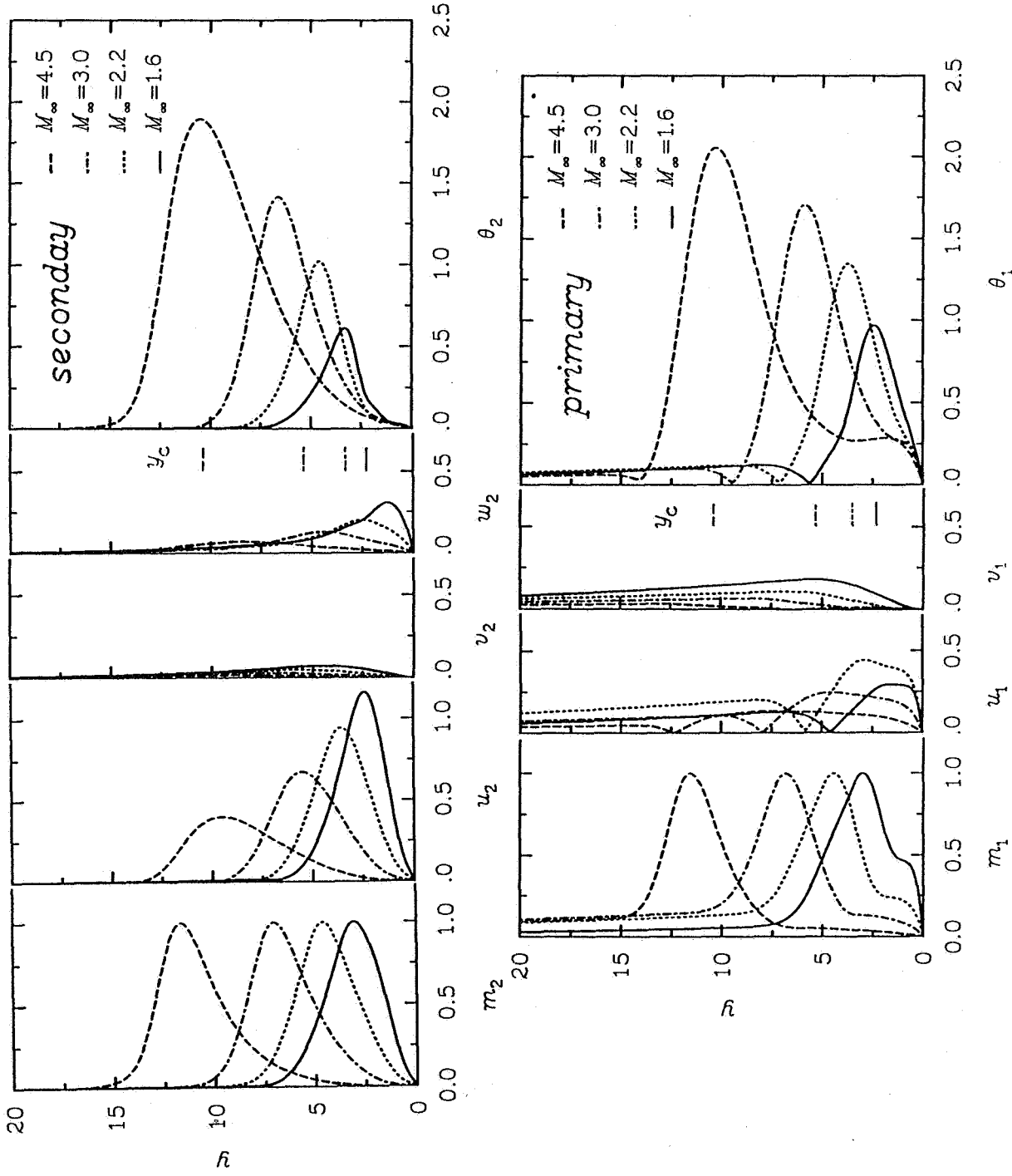
Figure 2 Variation across the boundary layer of the primary 2D first mode and the secondary subharmonic eigenfunctions at different Mach numbers, and the conditions of Figure 1 with $b = 0.18$.
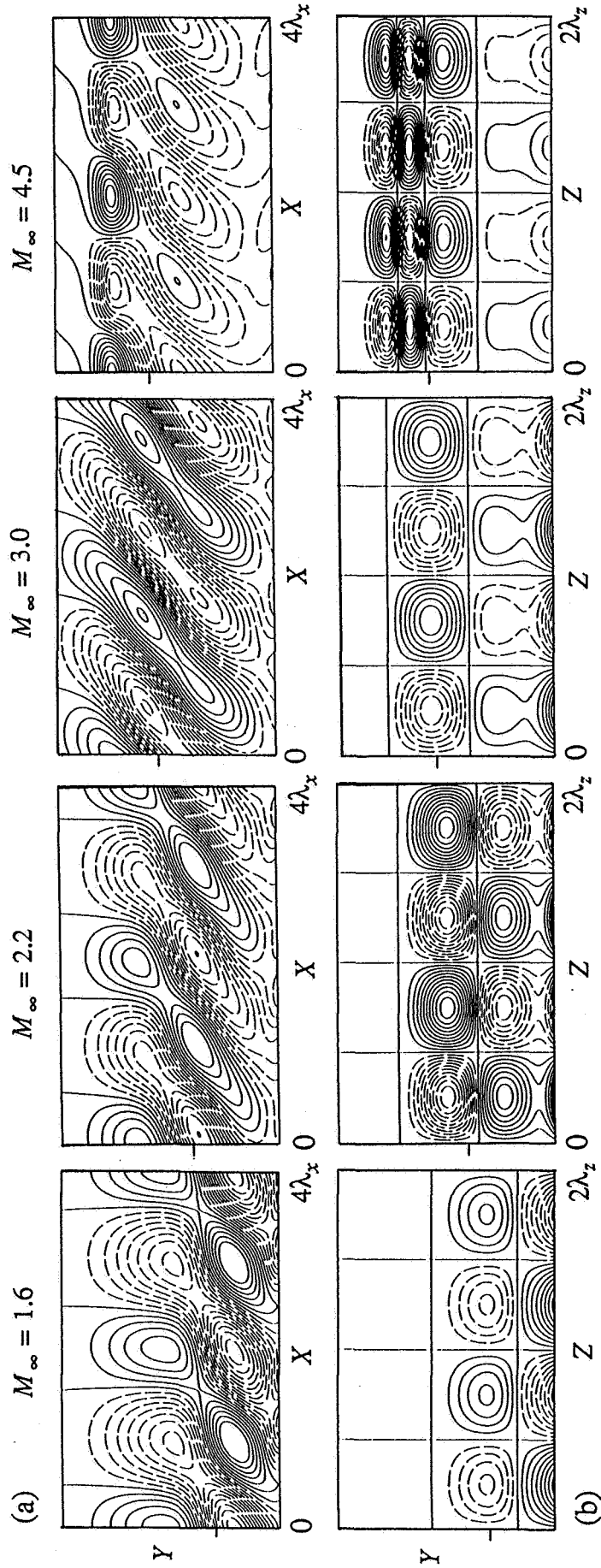
Figure 3 Vorticity contours of the total 3D flow at four different Mach numbers for the conditions of Figure 1 (broken lines indicate negative vorticity). The primary wave is a 2D first mode. (a) spanwise contours in the x–y plane at z=0, (b) streamwise contours in the z–y plane at x=0.
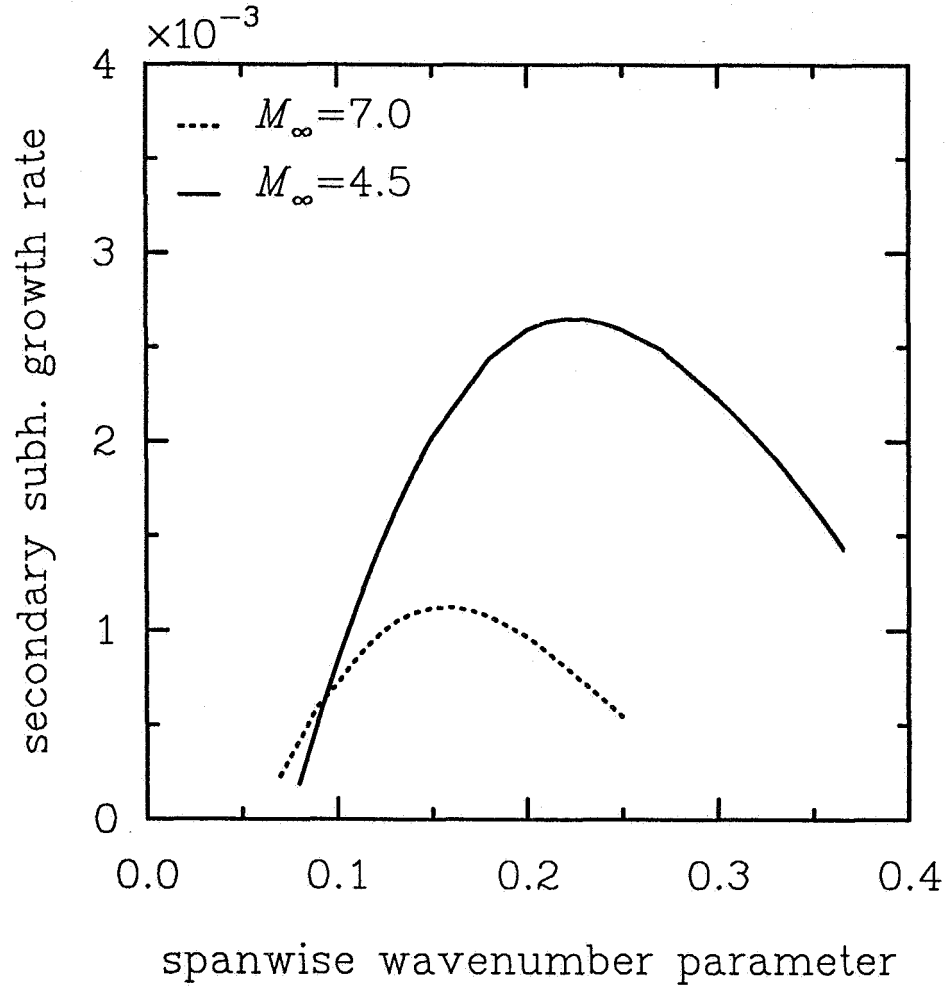
Figure 4 Effect of Mach number on the growth rate and the unstable band of the spanwise wavenumbers of the secondary subharmonic due to a 2D second mode primary wave at $R = 1000$, $F = 200$ for $M_\infty = 4.5$, $F = 180$ for $M_\infty = 7.0$, $A_m = 0.06$, and $\theta_\infty = 120K$.
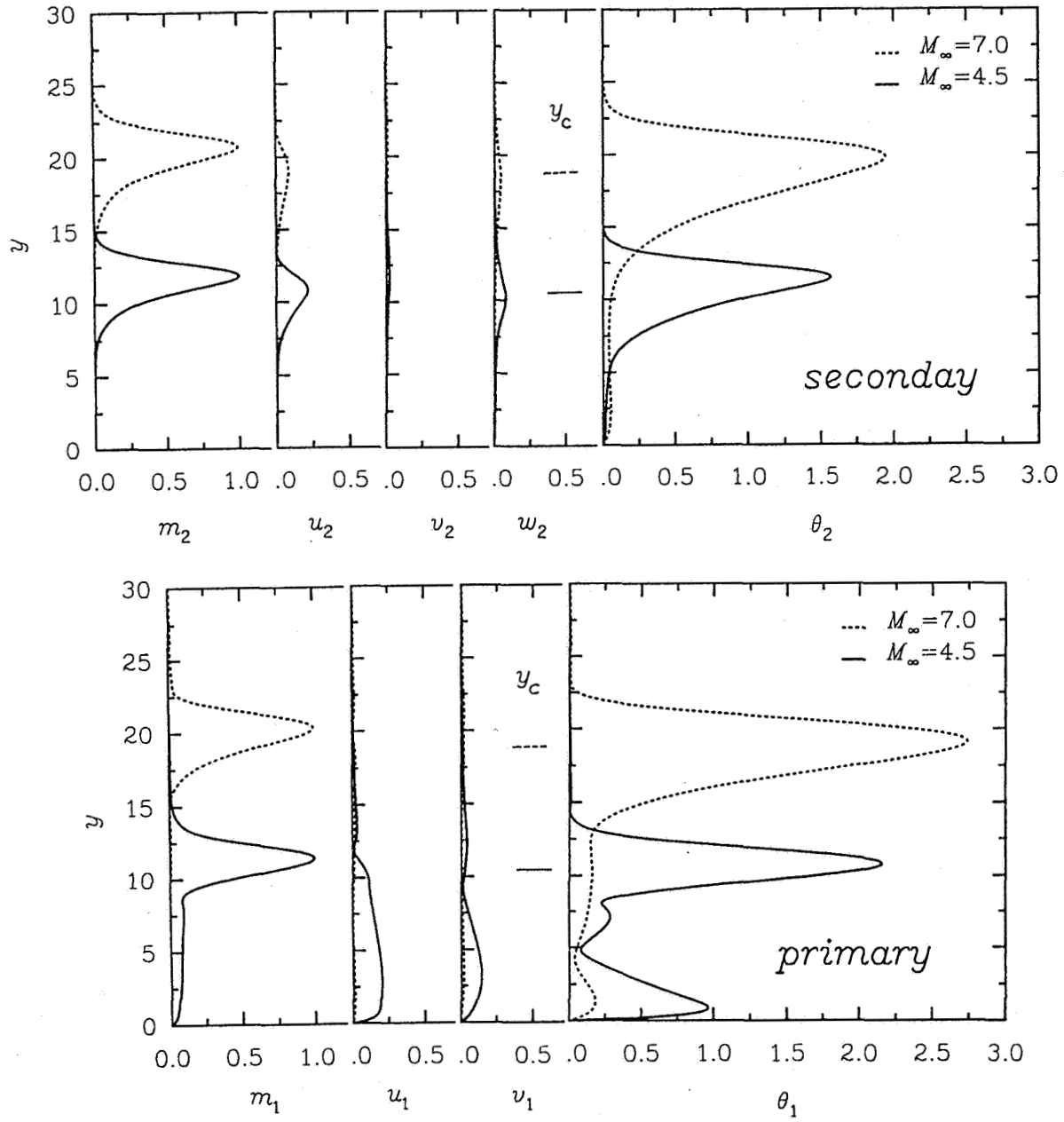
Figure 5 Variation across the boundary layer at hypersonic speeds of the primary 2D second mode and the secondary subharmonic eigenfunctions at the most unstable spanwise wavenumber (b=0.22 at M_∞=4.5, and b=0.15 at M_∞=7.0) and the conditions of Figure 4.
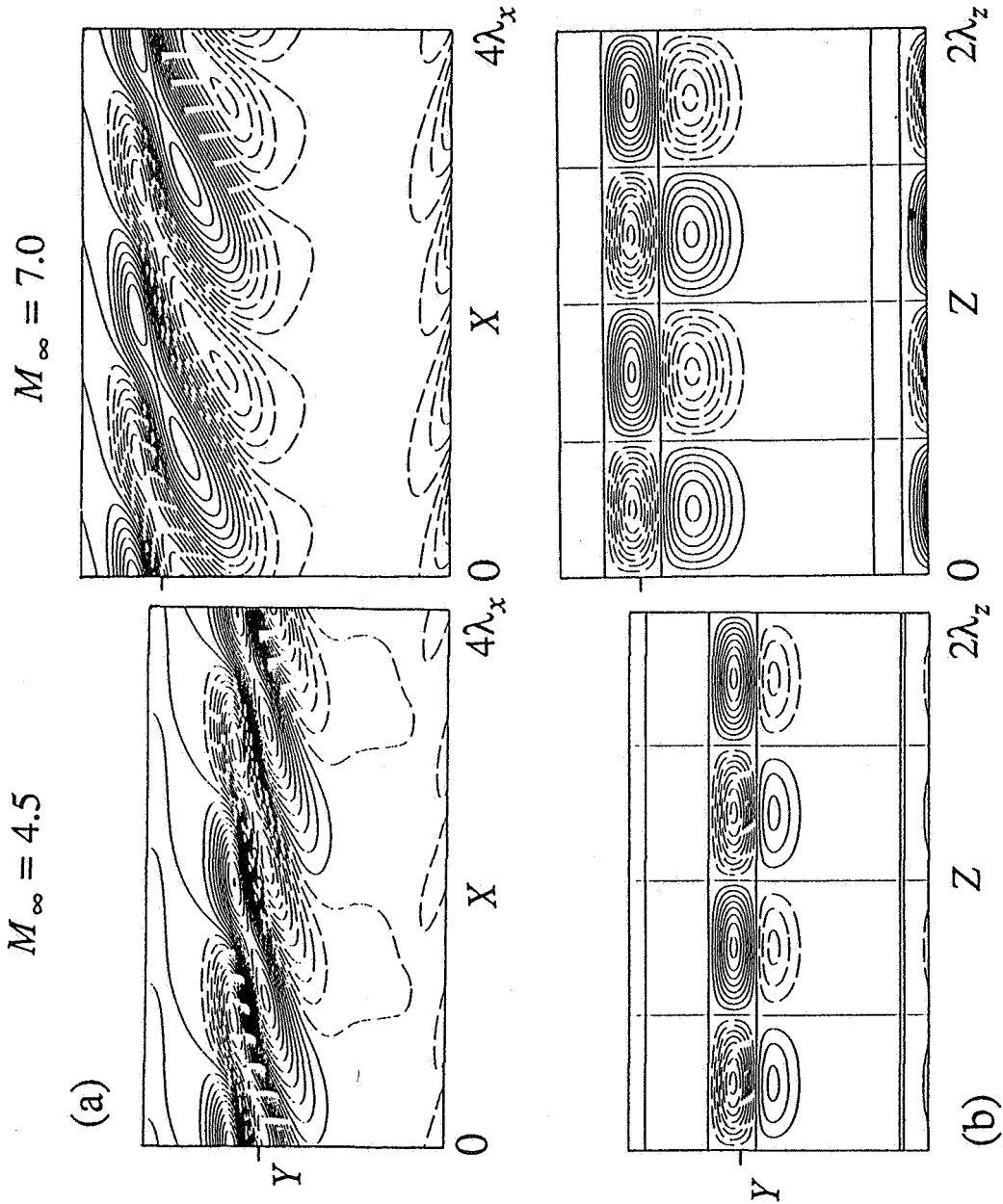
Figure 6 Contours of constant angular momentum components of the total 3D flow at hypersonic speeds and the conditions of Figure 4 (broken lines indicate negative vorticity). The primary wave is a 2D second mode. (a) spanwise contours in the $x–y$ plane at $z=0$, (b) streamwise contours in the $z–y$ plane at $x=0$.
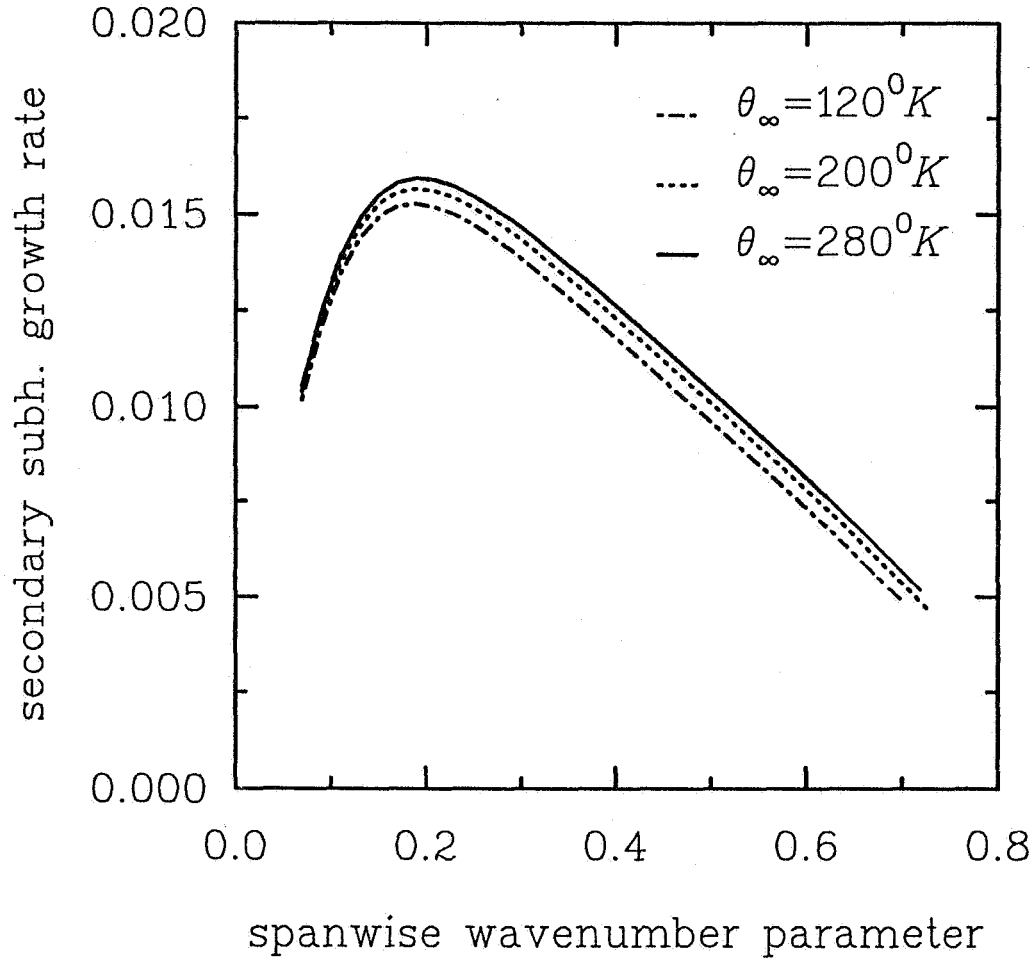
Figure 7(a) Effect of the free-stream temperature on the growth rate and the unstable band of spanwise wavenumbers of the secondary subharmonics. $M_\infty = 1.6$, $R = 800$, $F = 60$, $A_m = 0.06$, and the primary wave is 2D first mode.
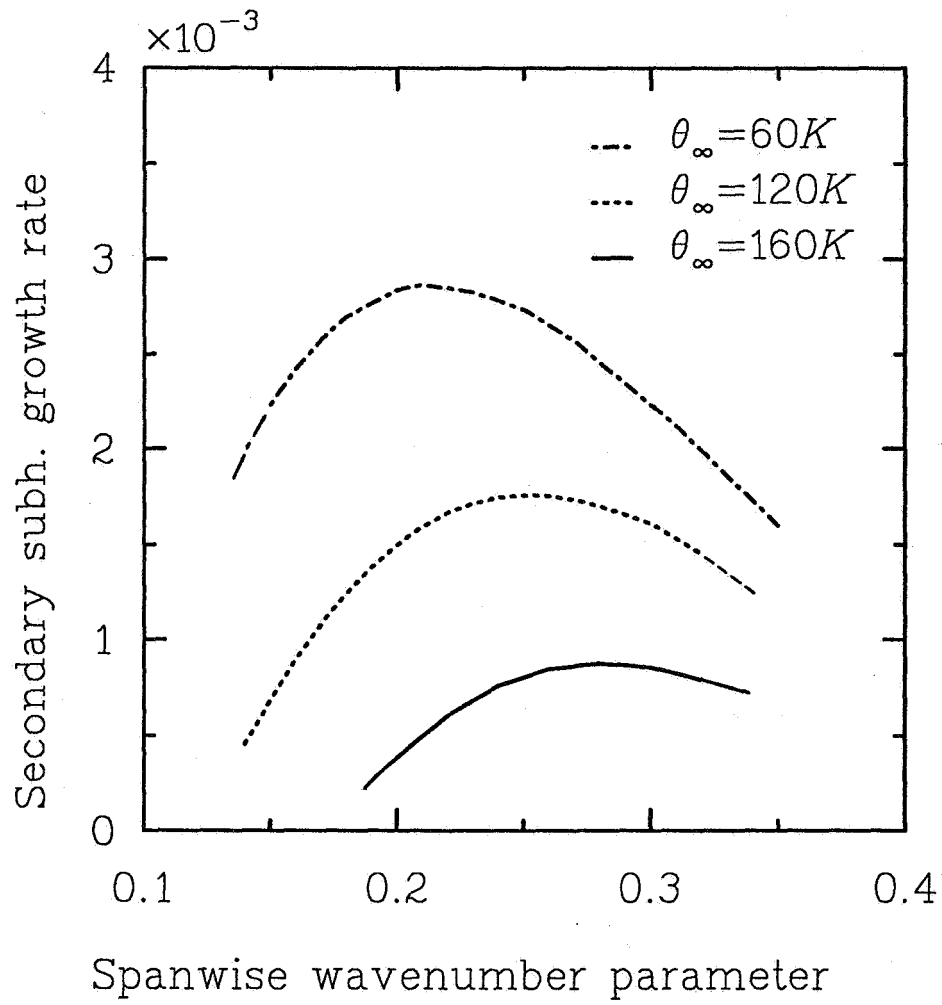
Figure 7(b) Effect of the free-stream temperature on the growth rate and the unstable band of spanwise wavenumbers of the secondary subharmonics. $M_\infty = 4.5$, $R = 956$, $F = 227$, $A_m = 0.023$, and the primary wave is 2D second mode.
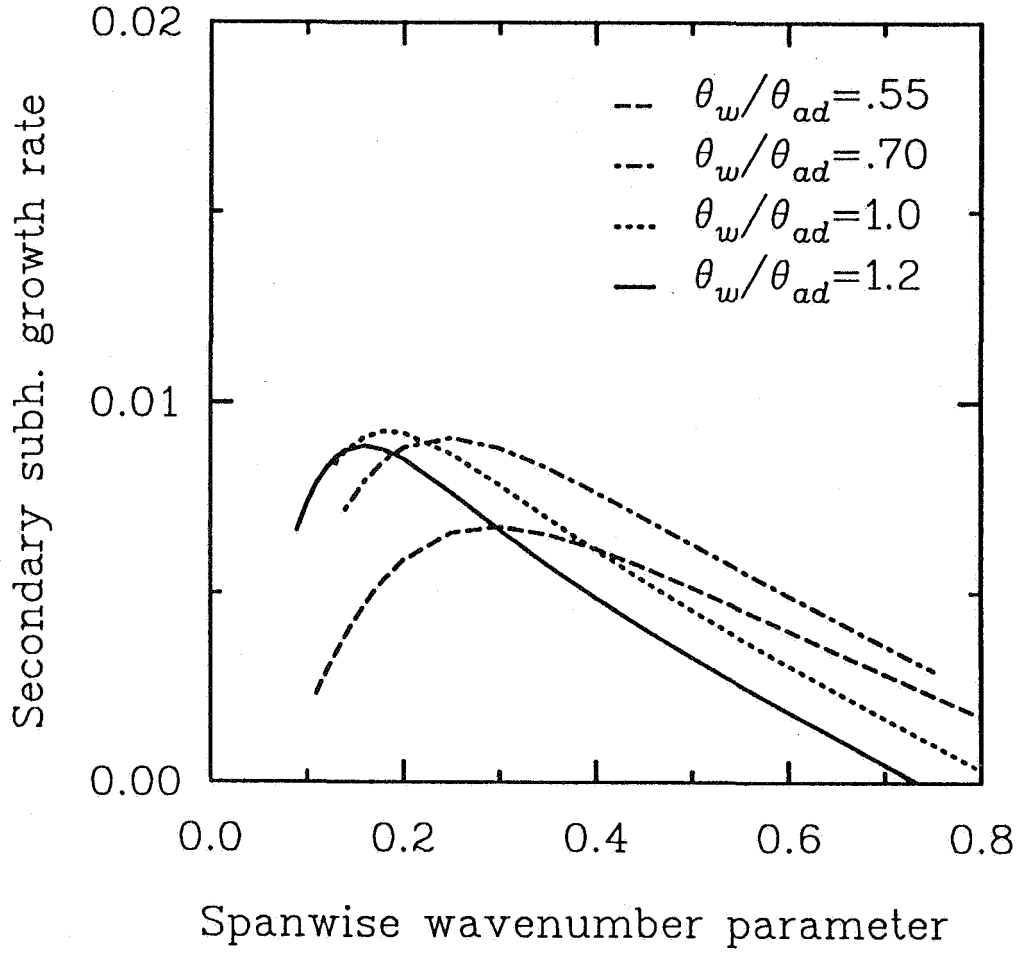
Figure 8(a) The local effect of wall cooling and heating on the growth rate and the unstable band of spanwise wavenumbers of the secondary subharmonics. $M_\infty = 0.8$, $R = 950$, $F = 60$, $A_m = 0.02$, $\theta_\infty = 275K$, and the primary wave is a 2D first mode.
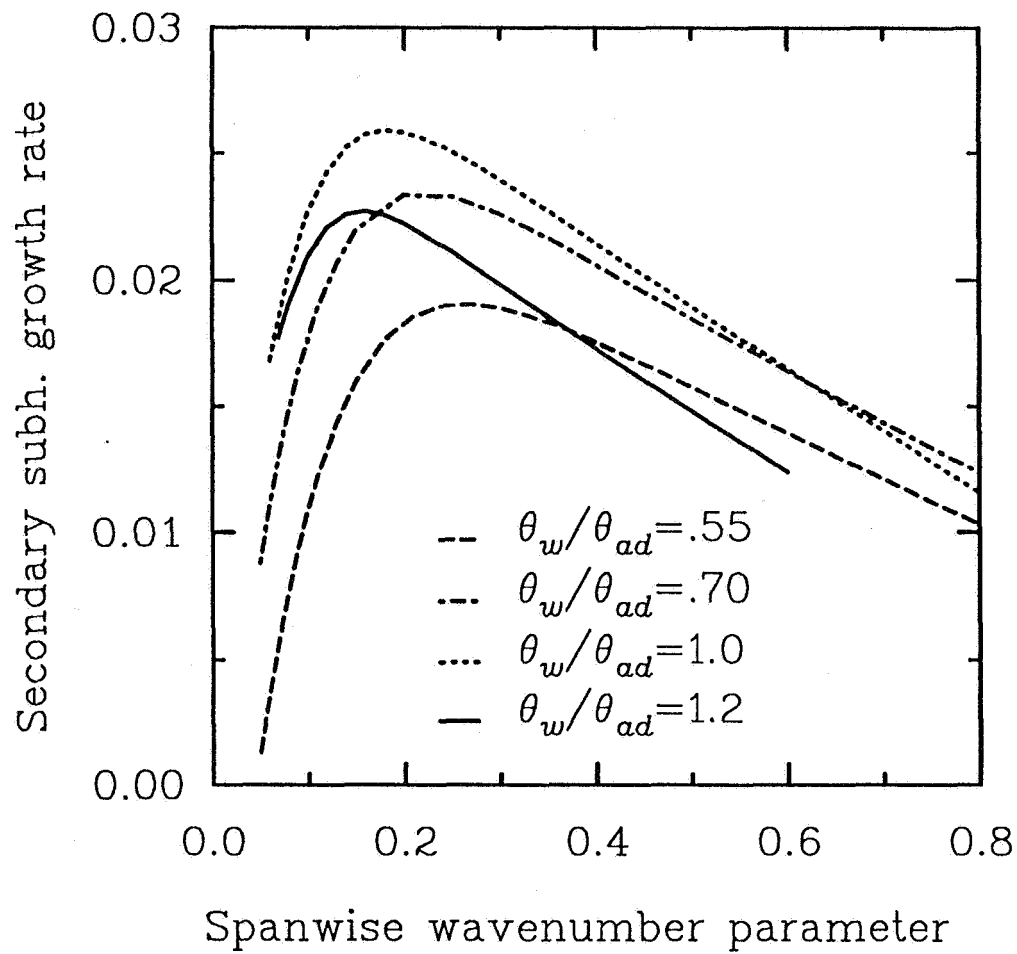
Figure 8(b) The local effect of wall cooling and heating on the growth rate and the unstable band of spanwise wavenumbers of the secondary subharmonics. $M_\infty = 1.6$, $R = 750$, $F = 60$, $A_m = 0.02$, $\theta_\infty = 205K$, and the primary wave is a 2D first mode.
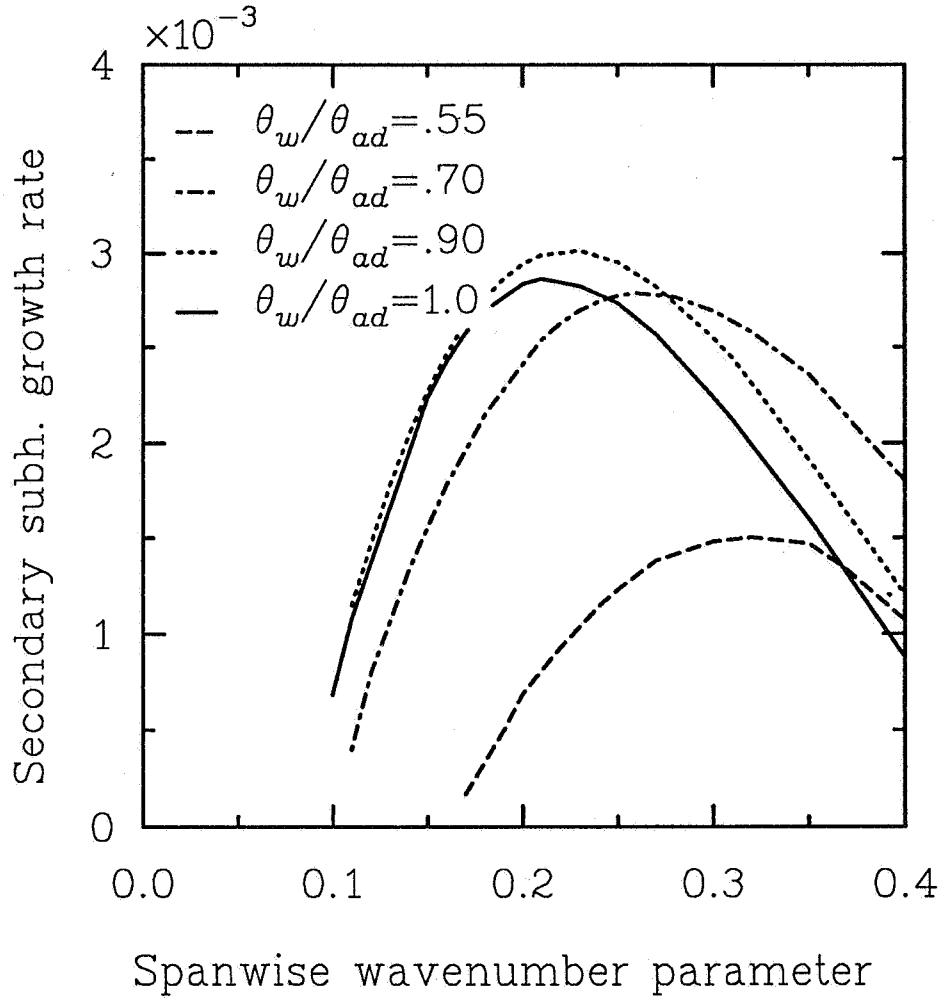
Figure 8(c) The local effect of wall cooling and heating on the growth rate and the unstable band of spanwise wavenumbers of the secondary subharmonics. $M_\infty = 4.5$, $R = 956$, $F = 227$, $A_m = 0.023$, $\theta_\infty = 62K$, and the primary wave is a 2D second mode.

41
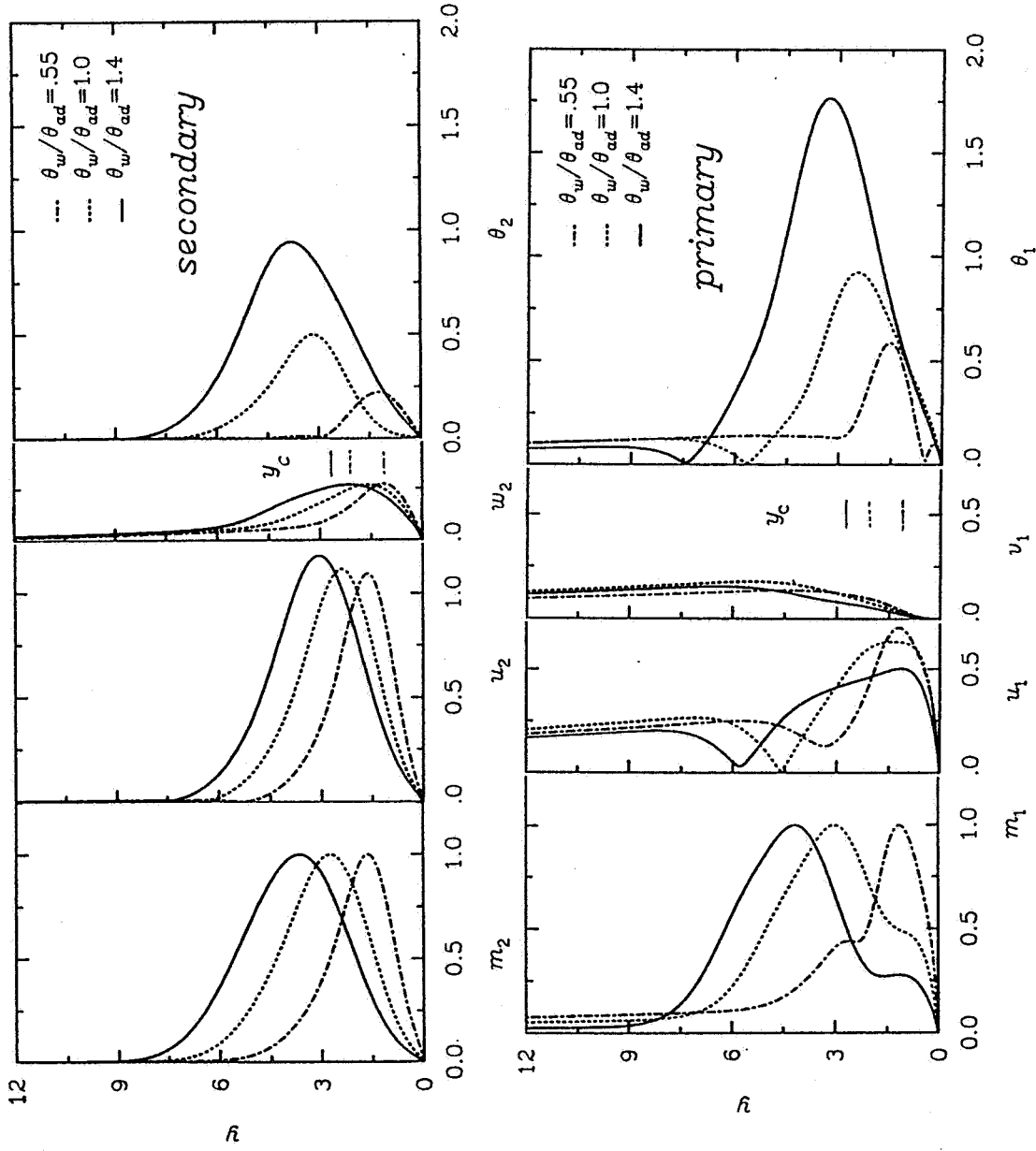
Figure 9 Effect of wall cooling and heating on the variation across the boundary layer of the primary 2D first mode and the secondary subharmonic eigenfunctions at $M_\infty = 1.6$, $R = 750$, $F = 60$, $A_m = 0.02$, $b = 0.2$, and $\theta_\infty = 205K$.
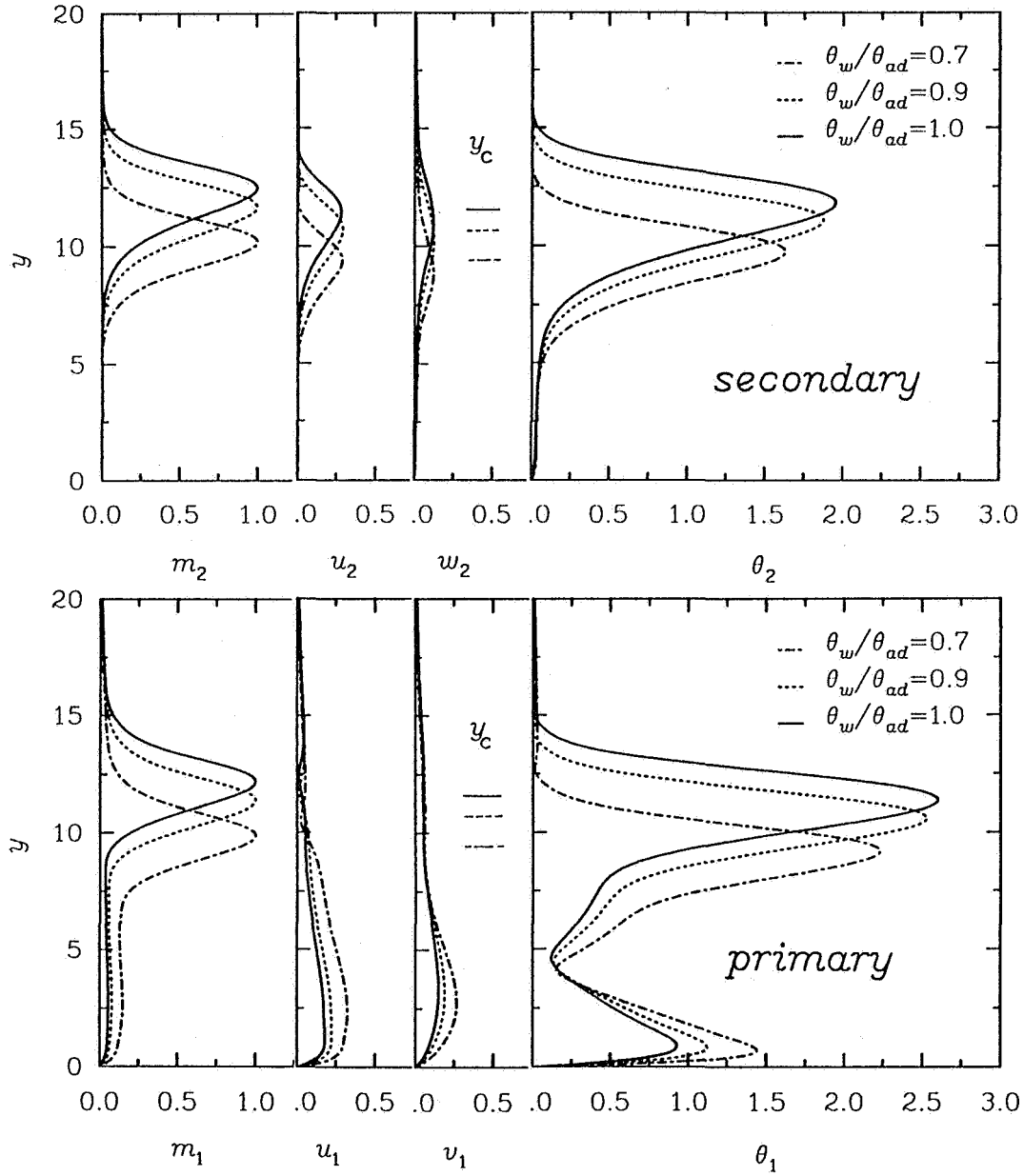
Figure 10 Effect of wall cooling on the variation across the boundary layer of the primary 2D second mode and the secondary subharmonic eigenfunctions at $M_\infty = 4.5$, $R = 956$, $F = 227$, $A_m = 0.023$, $b = 0.25$, and $\theta_\infty = 62K$.

43
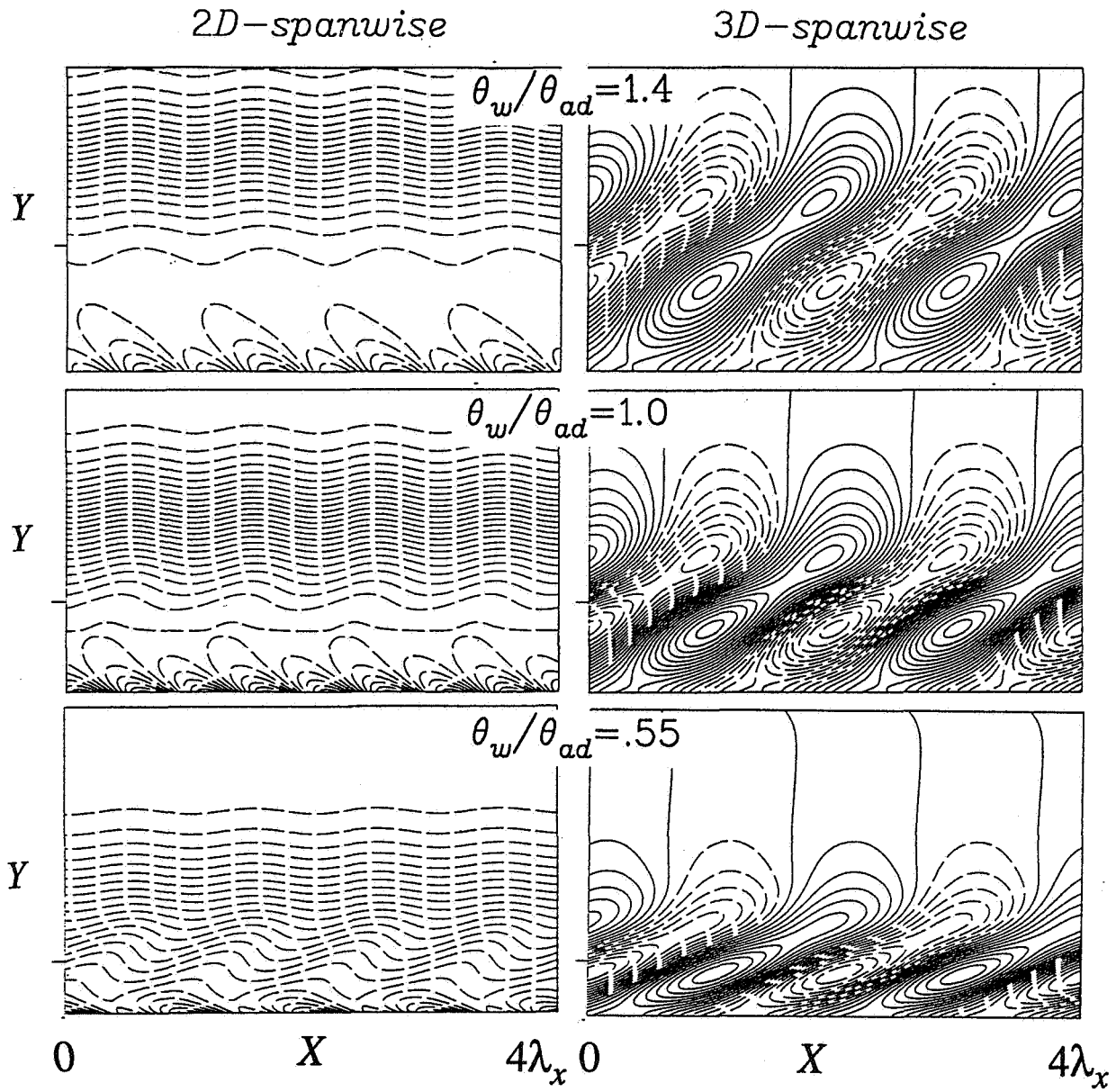
Figure 11 Effect of wall cooling and wall heating on the contours of the 2D-spanwise component and the 3D-spanwise component of the angular momentum at $M_\infty = 1.6$, and the conditions of Figure 12. The $x-y$ plane is at $z=0$, and the primary wave is a 2D first mode.
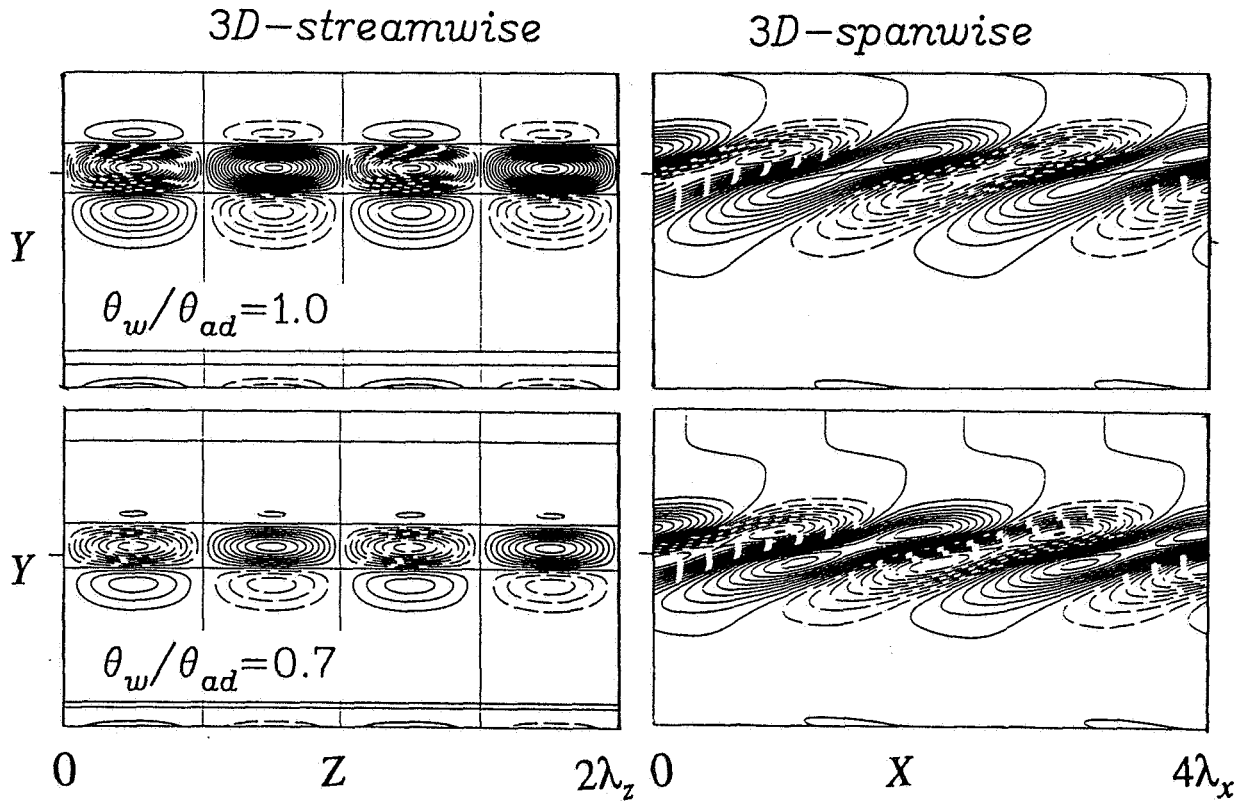
Figure 12 Effect of wall cooling on the contours of the streamwise and spanwise components of the angular momentum of the total 3D flow field at $M_\infty = 4.5$, and the conditions of Figure 13. The $x-y$ plane is at $z=0$, the $z-y$ plane is at $x=0$, and the primary wave is a 2D second mode.
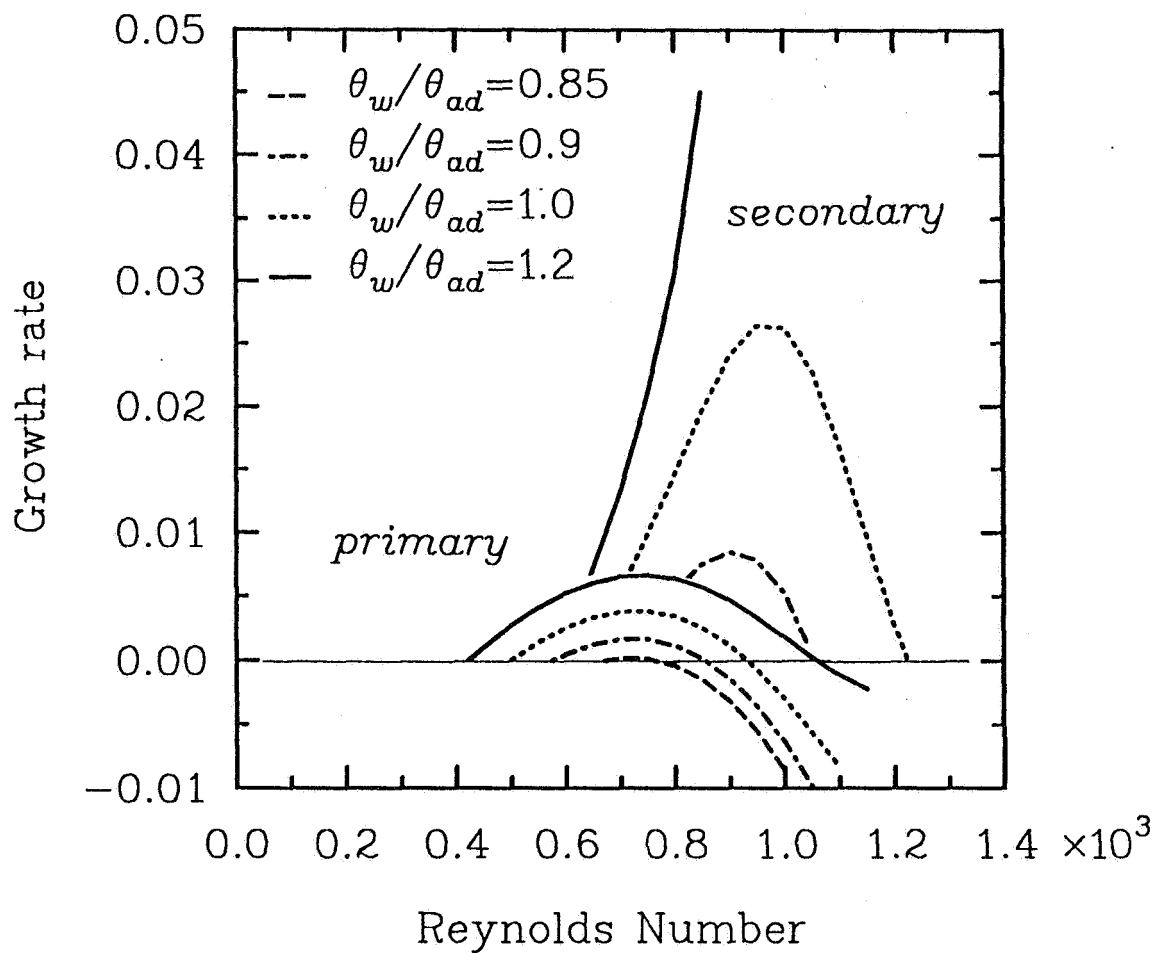
Figure 13(a) The overall effect of wall cooling and heating on the growth rates of the 2D first mode primary wave and the secondary subharmonic. Marching downstream includes the influence of increasing both A and R. $M_\infty = 0.8$, $F = 60$, $b = 0.2$, and the initial amplitude of the primary wave $A_{0m} = 0.0023$.
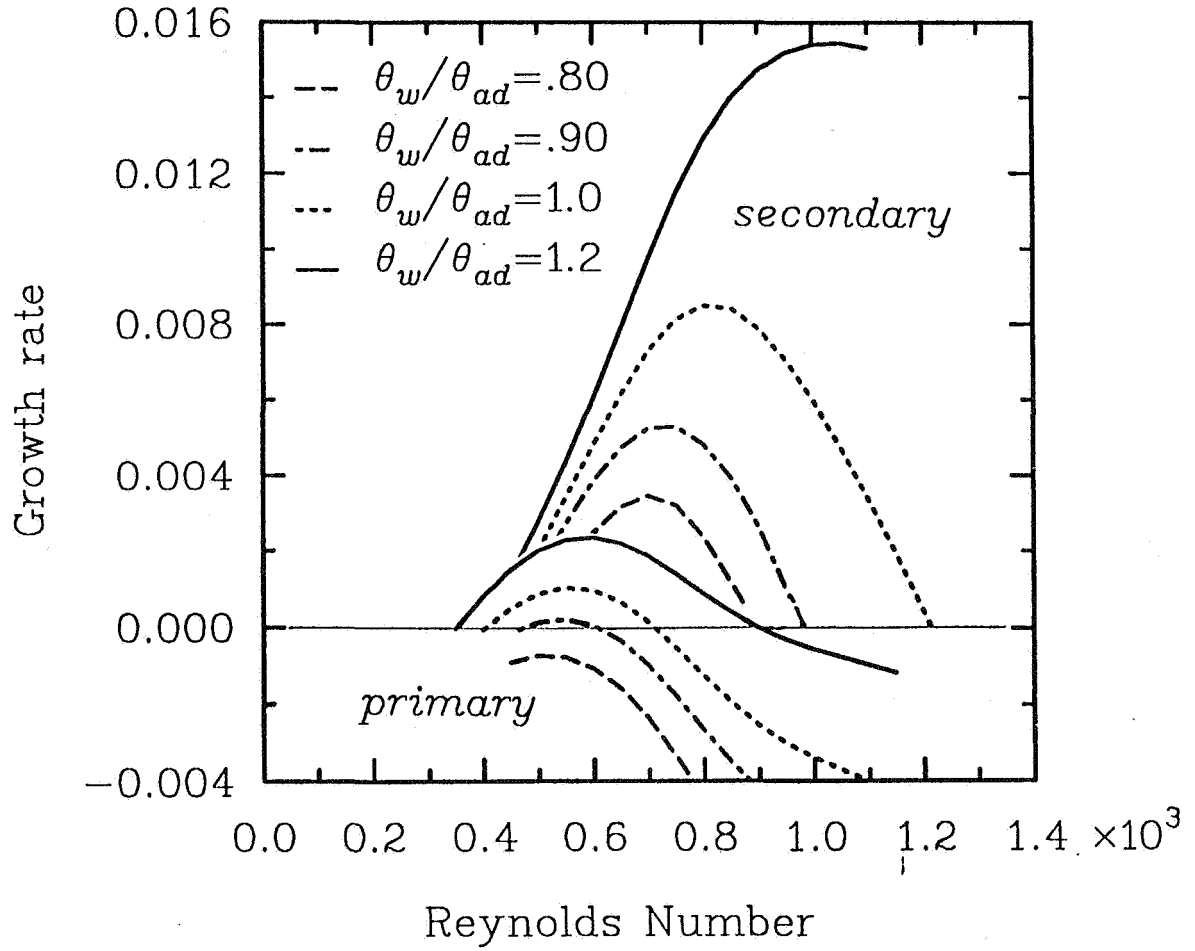
Figure 13(b) The overall effect of wall cooling and heating on the growth rates of the 2D first mode primary wave and the secondary subharmonic. Marching downstream includes the influence of increasing both A and R. $M_\infty = 1.6$, $F = 60$, $b = 0.2$, and the initial amplitude of the primary wave $A_{0m} = 0.01$.
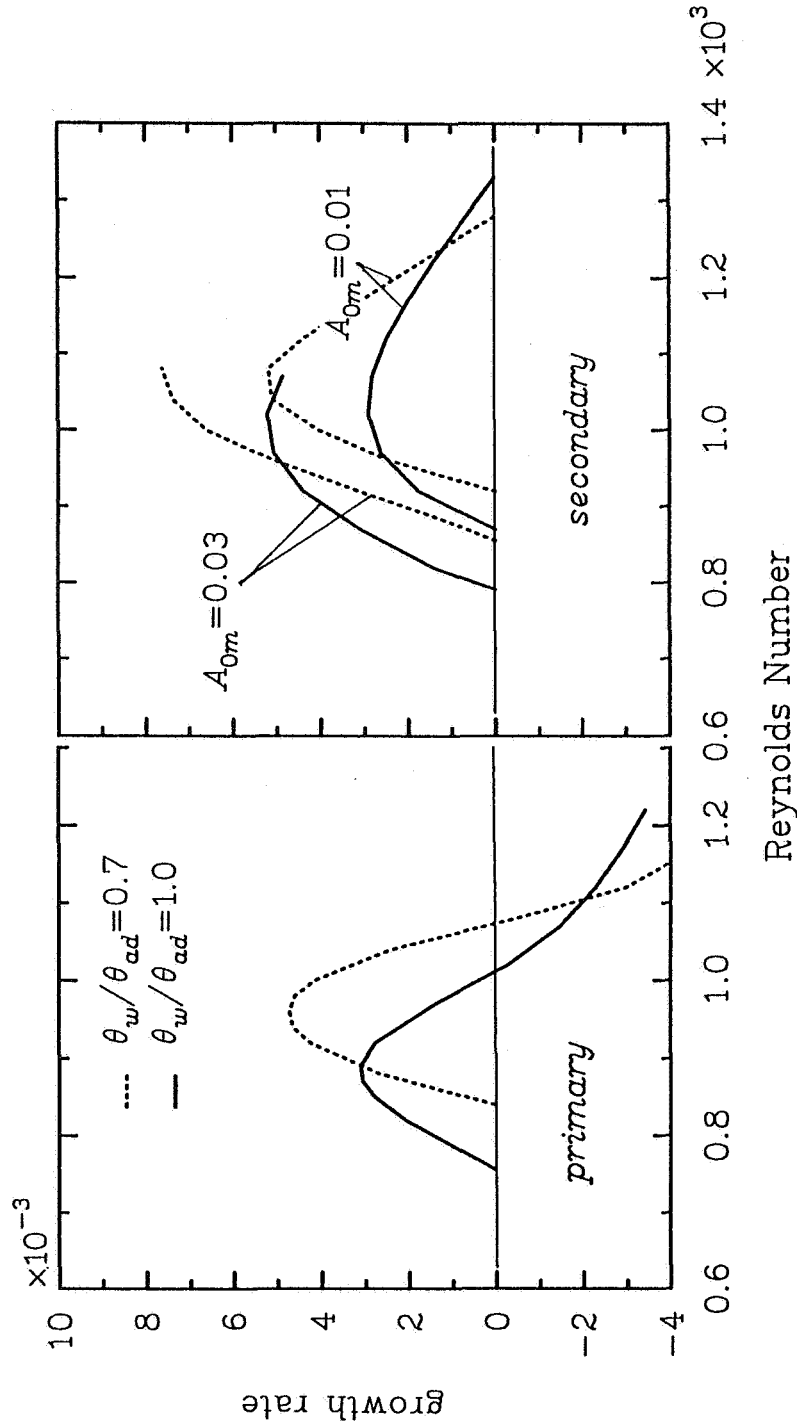
Figure 14 The overall effect of wall cooling on the growth rate of the 2D second mode primary wave and on the onset and growth rate of the secondary subharmonic at $M_\infty = 4.5$, $F = 227$, $b = 0.21$. Marching downstream includes the influence of increasing both A and R. The initial amplitudes of the primary wave are $A_{0m} = 0.01$ and $A_{0m} = 0.03$.
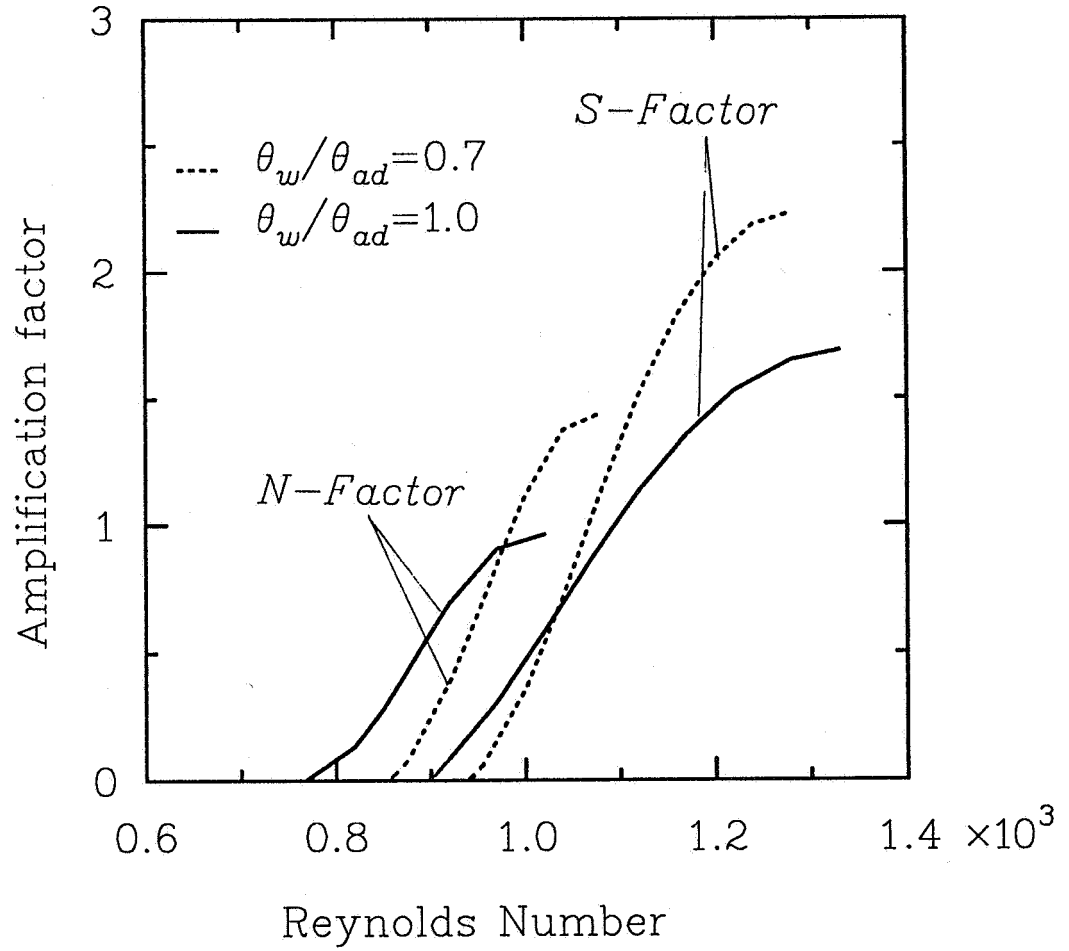
Figure 15 The overall effect of wall cooling on the N-factor of the 2D second mode primary wave and on the S-factor of the secondary subharmonic at $M_\infty = 4.5$, $F = 227$, $b = 0.21$. Marching downstream includes the influence of increasing both A and R. The initial amplitudes of the primary wave are $A_{0m} = 0.01$ and $A_{0m} = 0.03$.
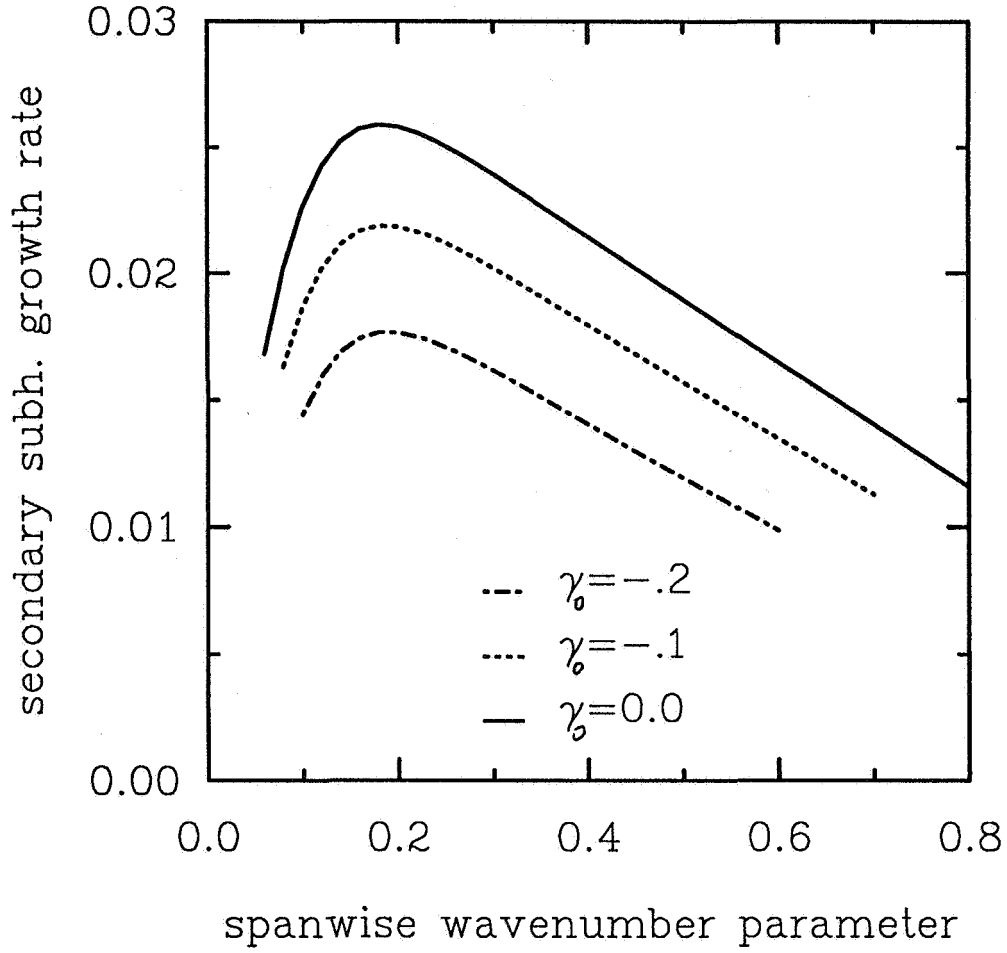
Figure 16(a) The local effect of wall suction on the growth rate and the unstable band of the spanwise wavenumbers of the secondary subharmonics. $M_\infty = 0.8$, $R = 950$, $F = 60$, $A_m = 0.02$, $\theta_\infty = 275K$, and the primary wave is a 2D first mode.
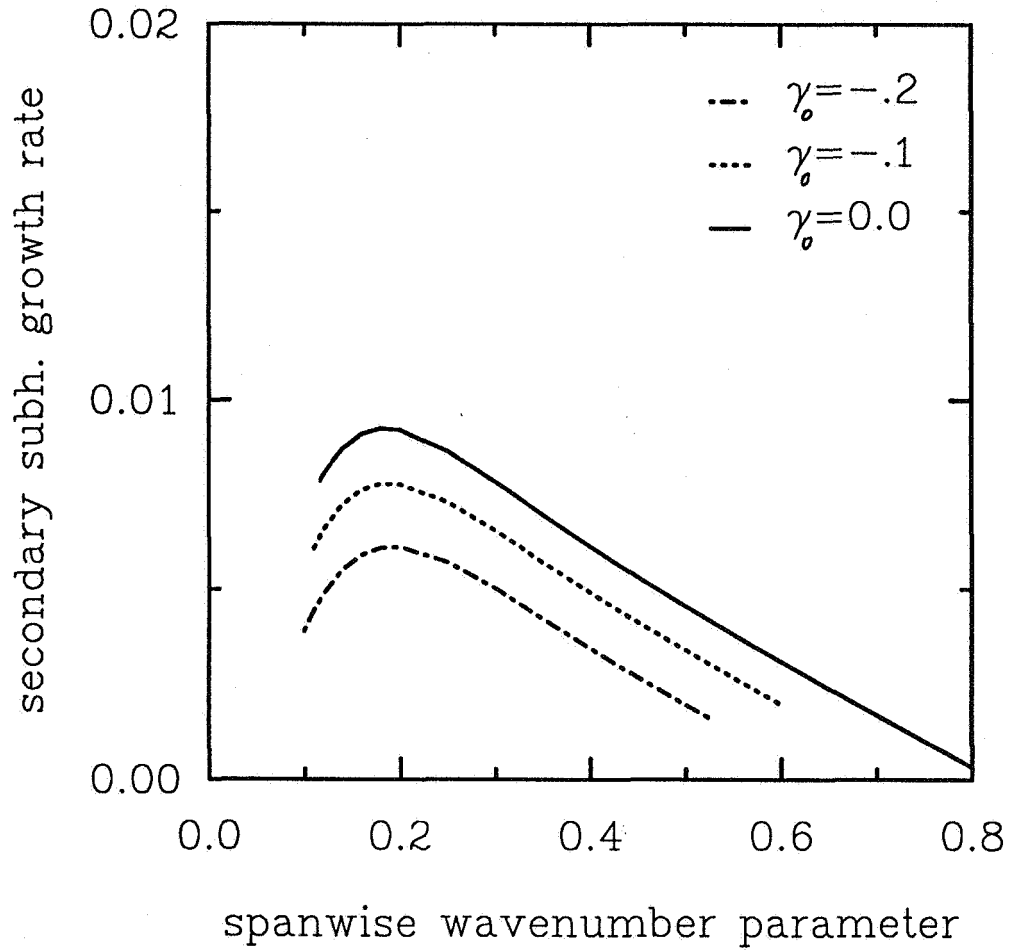
Figure 16(b) The local effect of wall suction on the growth rate and the unstable band of the spanwise wavenumbers of the secondary subharmonics. $M_\infty = 1.6$, $R = 750$, $F = 60$, $A_m = 0.02$, $\theta_\infty = 205K$, and the primary wave is a 2D first mode.
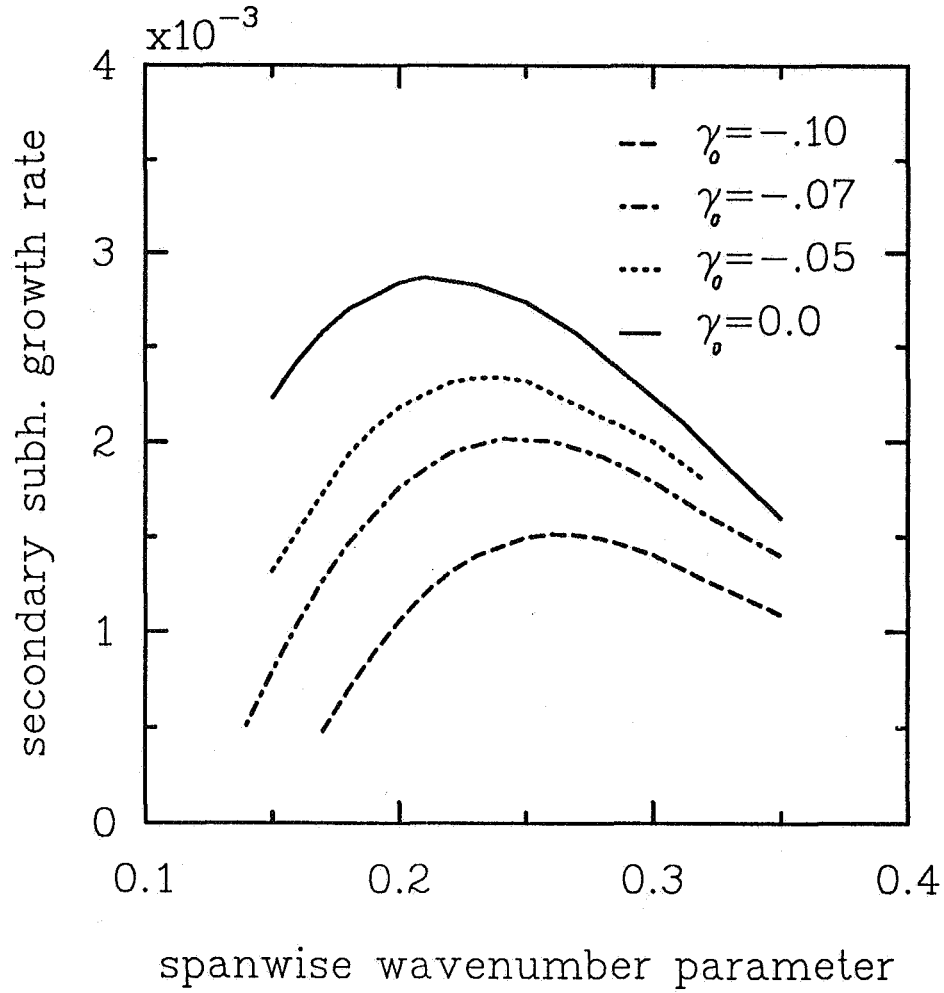
Figure 16(c) The local effect of wall suction on the growth rate and the unstable band of the spanwise wavenumbers of the secondary subharmonics. $M_\infty = 4.5$, $R = 956$, $F = 227$, $A_m = 0.023$, $\theta_\infty = 62K$, and the primary wave is a 2D second mode.
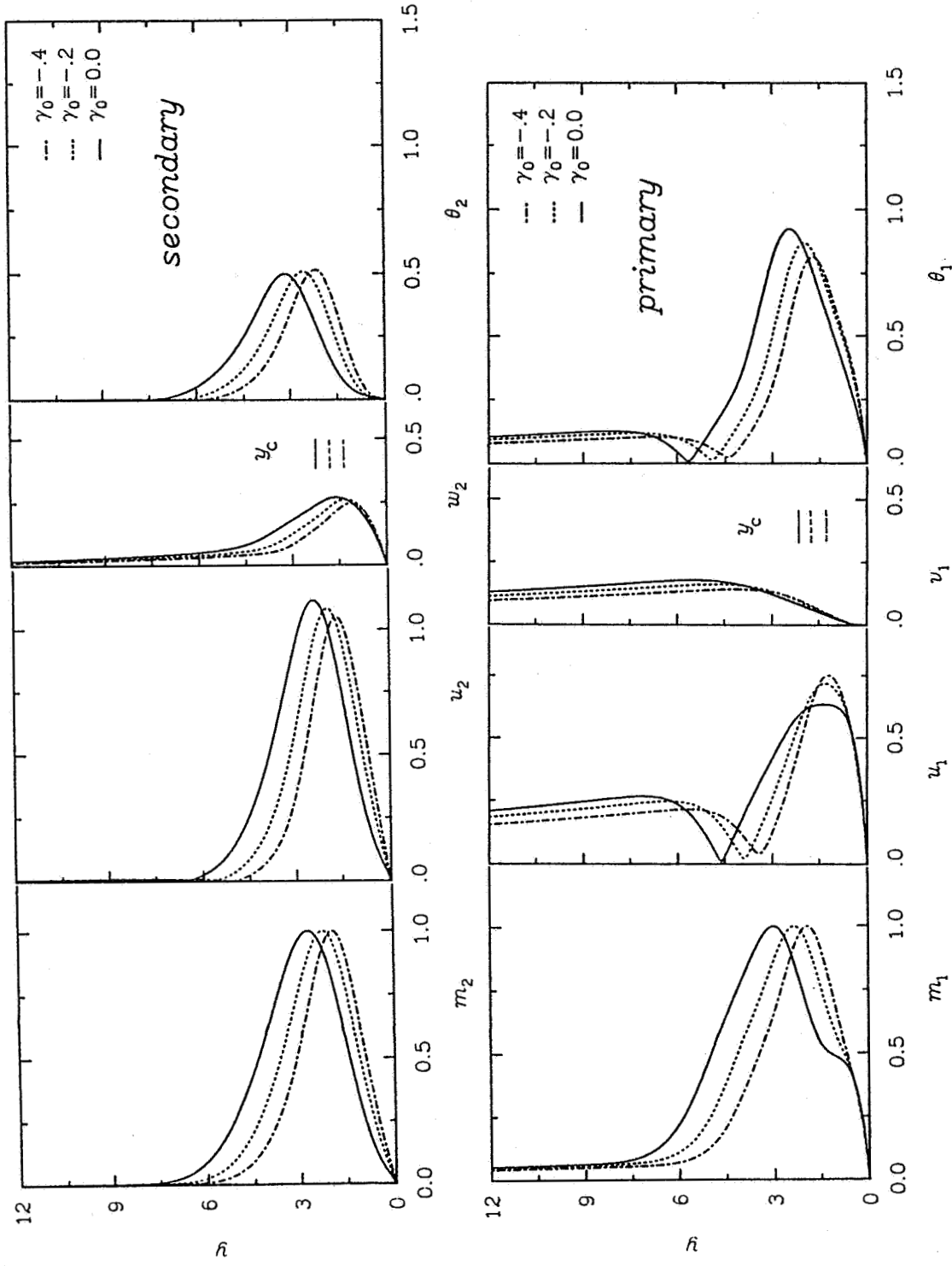
Figure 17 Effect of suction on the variation across the boundary layer of the primary 2D first mode and the secondary subharmonic eigenfunctions at $M_\infty = 1.6$, $R = 750$, $F = 60$, $A_m = 0.02$, $b = 0.2$, and $\theta_\infty = 205K$.
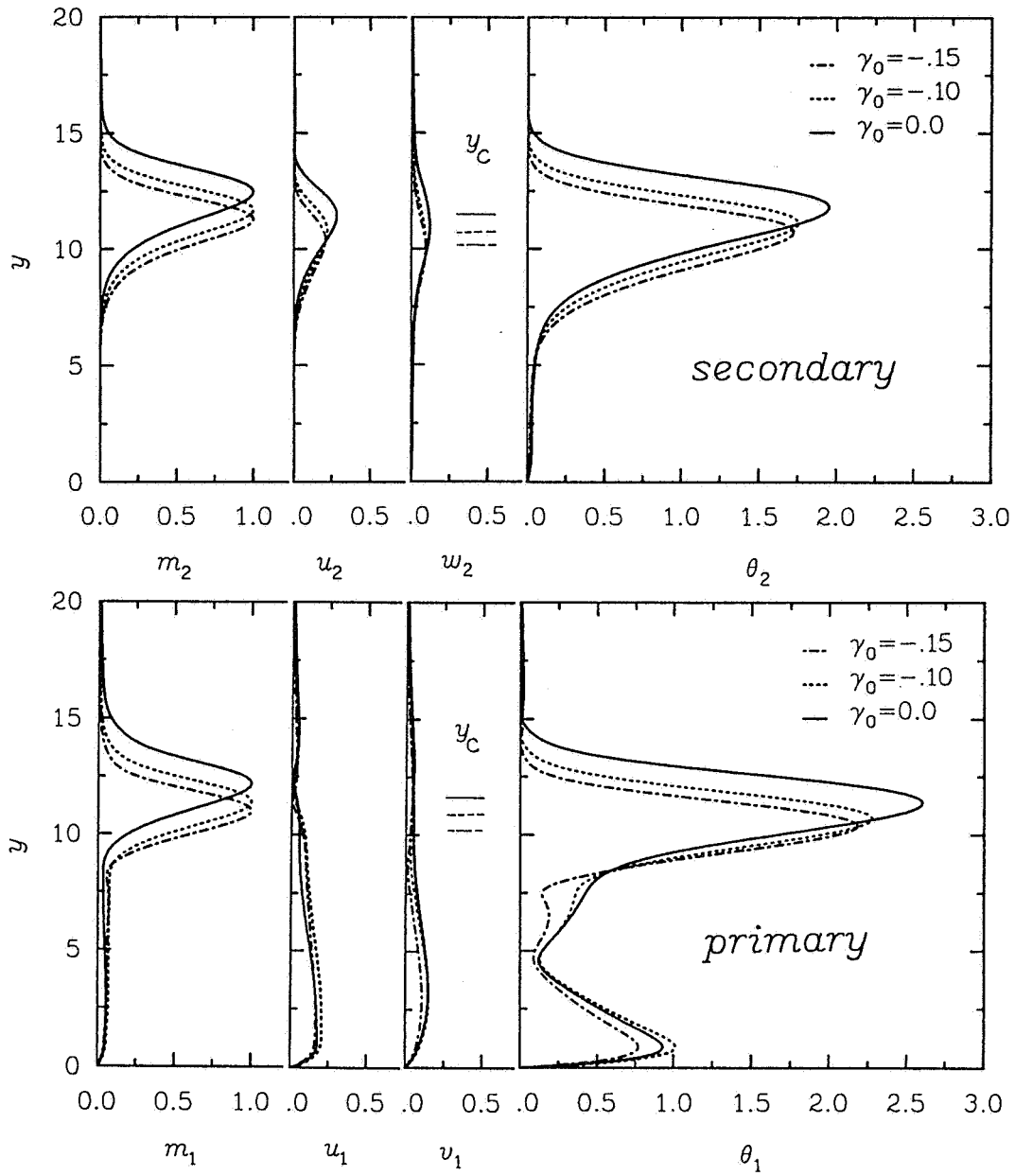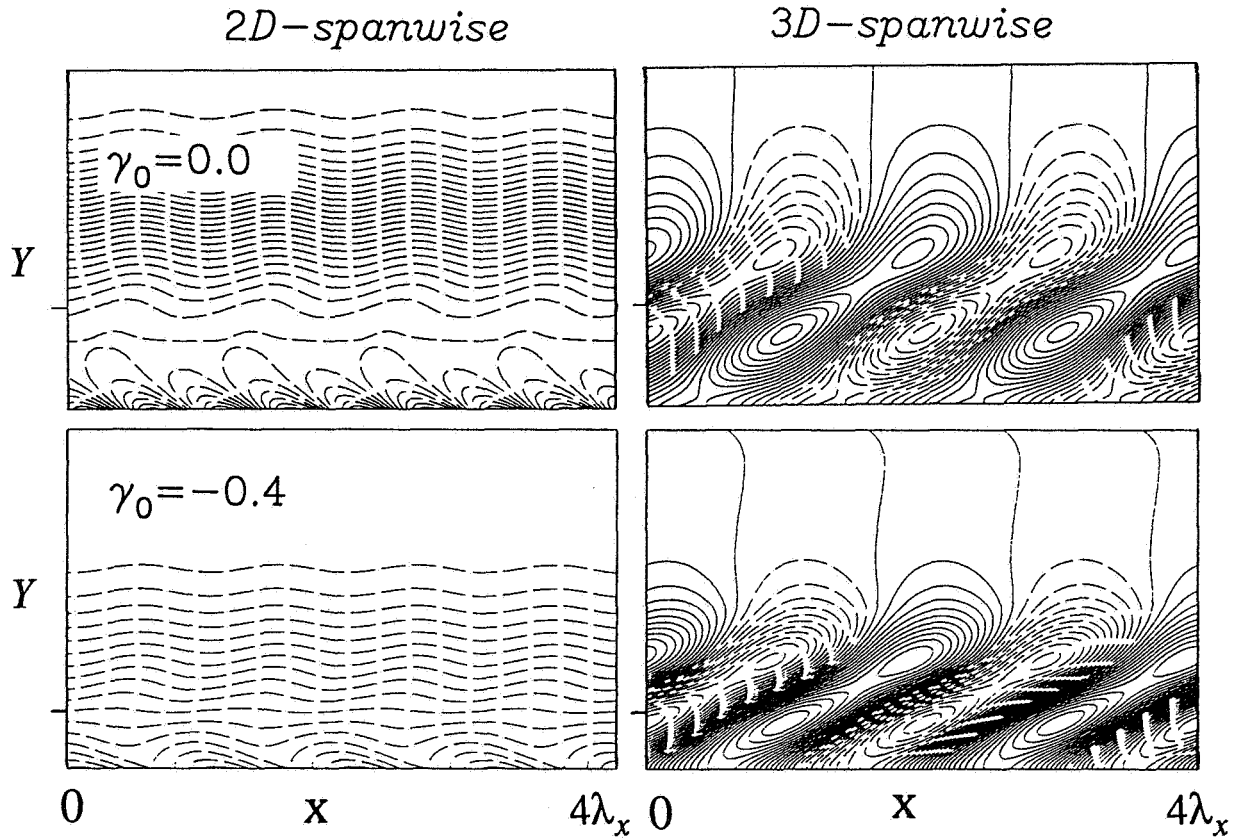
Figure 18 Effect of suction on the variation across the boundary layer of the primary 2D second mode and the secondary subharmonic eigenfunctions at $M_\infty = 4.5$, $R = 956$, $F = 227$, $A_m = 0.023$, $b = 0.25$, and $\theta_\infty = 62K$.

Figure 19 Effect of suction on the contours of the 2D-spanwise component and the 3D-spanwise component of the angular momentum at $M_\infty = 1.6$, and the conditions of Figure 16. The x–y plane is at z=0, and the primary wave is a 2D first mode.
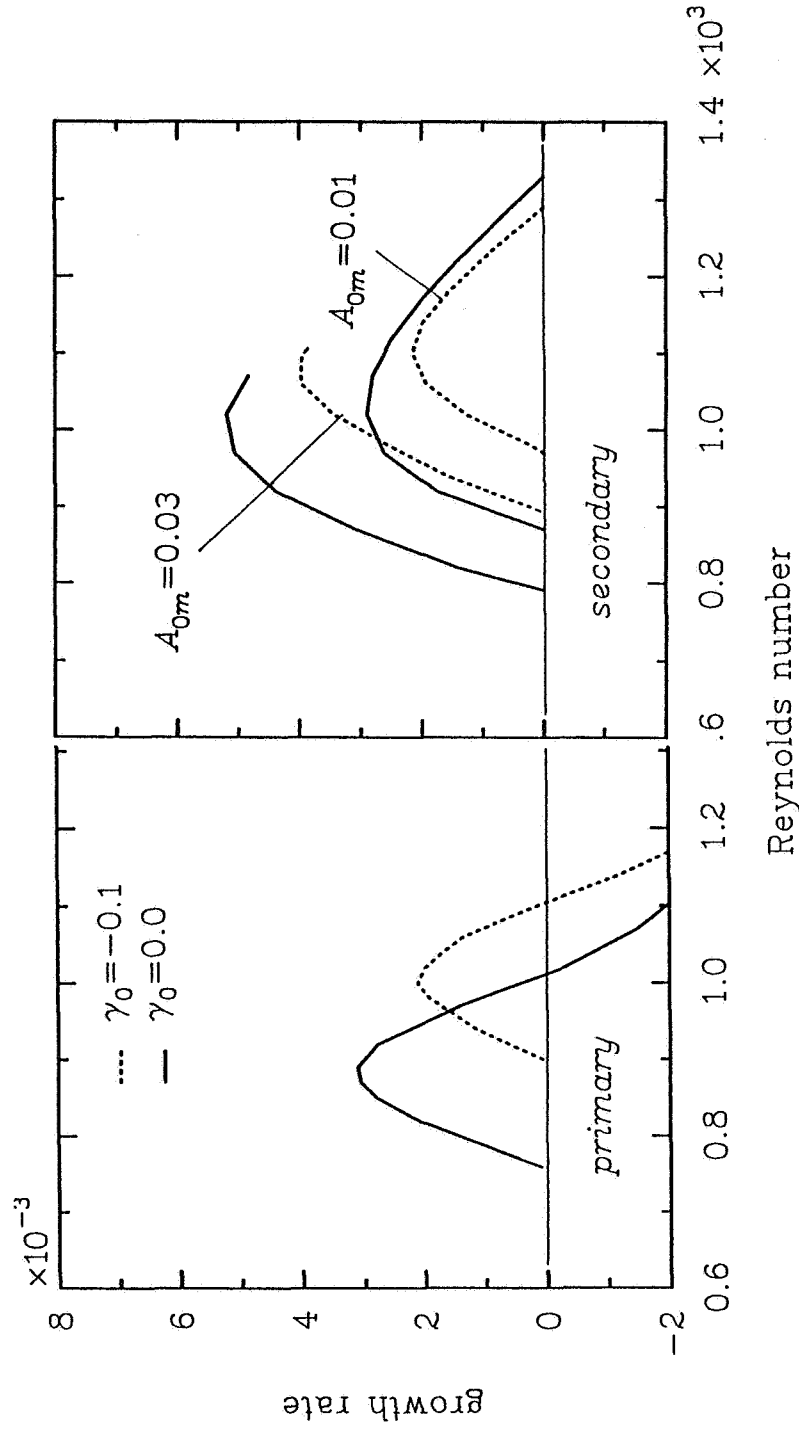
Figure 20 The overall effect of suction on the growth rate of the 2D second mode primary wave and on the onset and growth rate of the secondary subharmonic at $M_\infty = 4.5$, $F = 227$, $b = 0.21$. Marching downstream includes the influence of increasing both A and R. The initial amplitudes of the primary wave are $A_{0m} = 0.01$ and $A_{0m} = 0.03$.

REPORT DOCUMENTATION PAGE

1. AGENCY USE ONLY (Leave blank)	2. REPORT DATE February 1992	3. REPORT TYPE AND DATES COVERED Contractor Report

4. TITLE AND SUBTITLE

Secondary Instability of High-Speed Flows and the Influence of Wall Cooling and Suction

6. AUTHOR(S)

Nabil M. El-Hady

5. FUNDING NUMBERS

C NAS1-18599

WU 505-59-50-01

7. PERFORMING ORGANIZATION NAME(S) AND ADDRESS(ES)

Analytical Services and Materials, Inc.
Hampton, VA 23666

8. PERFORMING ORGANIZATION REPORT NUMBER

9. SPONSORING/MONITORING AGENCY NAME(S) AND ADDRESS(ES)

National Aeronautics and Space Administration
Langley Research Center
Hampton, VA 23665-5225

10. SPONSORING/MONITORING AGENCY REPORT NUMBER

NASA CR-4427

11. SUPPLEMENTARY NOTES

Langley Technical Monitor: Ajay Kumar

12a. DISTRIBUTION/AVAILABILITY STATEMENT

Unclassified - Unlimited

Subject Category 34

12b. DISTRIBUTION CODE

13. ABSTRACT (Maximum 200 words)

The periodic streamwise modulation of the supersonic and hypersonic boundary layers by a two-dimensional first-mode or second-mode wave makes the resulting base flow susceptible to a broad-band spanwise-periodic three-dimensional type of instability. The principal parametric resonance of this instability (subharmonic) has been analyzed using Floquet theory. The effect of Mach number and the effectiveness of wall cooling or wall suction in controlling the onset, the growth rate, and the vortical structure of the subharmonic secondary instability are assessed for both a first-mode and a second-mode primary wave. Results indicate that the secondary subharmonic instability of an insulated wall boundary layer is weakened as Mach number increases. Cooling of the wall destabilizes the secondary subharmonic of a second-mode primary wave, but stabilizes it when the primary wave is a first mode. Suction stabilizes the secondary subharmonic at all Mach numbers.

14. SUBJECT TERMS

secondary instability; high-speed boundary layer; boundary-layer control

15. NUMBER OF PAGES
56

16. PRICE CODE
A04

17. SECURITY CLASSIFICATION OF REPORT	18. SECURITY CLASSIFICATION OF THIS PAGE	19. SECURITY CLASSIFICATION OF ABSTRACT	20. LIMITATION OF ABSTRACT
Unclassified	Unclassified	Unclassified	Unlimited